

Evaluation of the Performance of A1010 Bridge Steel

Final Report
January 2020



IOWA STATE UNIVERSITY
Institute for Transportation

Sponsored by
Iowa Department of Transportation
(InTrans Project 16-562)

About BEC

The mission of the Bridge Engineering Center (BEC) is to conduct research on bridge technologies to help bridge designers/owners design, build, and maintain long-lasting bridges.

About InTrans

The mission of the Institute for Transportation (InTrans) at Iowa State University is to develop and implement innovative methods, materials, and technologies for improving transportation efficiency, safety, reliability, and sustainability while improving the learning environment of students, faculty, and staff in transportation-related fields.

ISU Nondiscrimination Statement

Iowa State University does not discriminate on the basis of race, color, age, ethnicity, religion, national origin, pregnancy, sexual orientation, gender identity, genetic information, sex, marital status, disability, or status as a US veteran. Inquiries regarding non-discrimination policies may be directed to the Office of Equal Opportunity, 3410 Beardshear Hall, 515 Morrill Road, Ames, Iowa 50011, Tel. 515-294-7612, hotline: 515-294-1222, email: eooffice@iastate.edu.

Disclaimer Notice

The contents of this report reflect the views of the authors, who are responsible for the facts and the accuracy of the information presented herein. The opinions, findings and conclusions expressed in this publication are those of the authors and not necessarily those of the sponsors.

The sponsors assume no liability for the contents or use of the information contained in this document. This report does not constitute a standard, specification, or regulation.

The sponsors do not endorse products or manufacturers. Trademarks or manufacturers' names appear in this report only because they are considered essential to the objective of the document.

Iowa DOT Statements

Federal and state laws prohibit employment and/or public accommodation discrimination on the basis of age, color, creed, disability, gender identity, national origin, pregnancy, race, religion, sex, sexual orientation or veteran's status. If you believe you have been discriminated against, please contact the Iowa Civil Rights Commission at 800-457-4416 or Iowa Department of Transportation's affirmative action officer. If you need accommodations because of a disability to access the Iowa Department of Transportation's services, contact the agency's affirmative action officer at 800-262-0003.

The preparation of this report was financed in part through funds provided by the Iowa Department of Transportation through its "Second Revised Agreement for the Management of Research Conducted by Iowa State University for the Iowa Department of Transportation" and its amendments.

The opinions, findings, and conclusions expressed in this publication are those of the authors and not necessarily those of the Iowa Department of Transportation.

Technical Report Documentation Page

1. Report No. InTrans Project 16-562	2. Government Accession No.	3. Recipient's Catalog No.	
4. Title Evaluation of the Performance of A1010 Bridge Steel		5. Report Date January 2020	
		6. Performing Organization Code	
7. Author(s) Brent Phares (orcid.org/0000-0001-5894-4774), Behrouz Shafei (orcid.org/0000-0001-5677-6324), and Weizhuo Shi (orcid.org/0000-0001-8193-0098)		8. Performing Organization Report No. InTrans Project 16-562	
9. Performing Organization Name and Address Bridge Engineering Center Iowa State University 2711 South Loop Drive, Suite 4700 Ames, IA 50010-8664		10. Work Unit No. (TRAIS)	
		11. Contract or Grant No.	
12. Sponsoring Organization Name and Address Iowa Department of Transportation 800 Lincoln Way Ames, IA 50010		13. Type of Report and Period Covered Final Report	
		14. Sponsoring Agency Code	
15. Supplementary Notes Visit www.intrans.iastate.edu for color pdfs of this and other research reports.			
16. Abstract <p>ASTM A1010 steel is a nominal 12% chromium (10.5% minimum and 12.5% maximum) steel reported to have enhanced corrosion resistance compared to traditional painted structural steels, weathering steels, and galvanized steels. In 2016, the Iowa Department of Transportation (DOT) built a four-span bridge partially constructed using A1010 steel.</p> <p>Despite the wealth of information on the durability of A1010 steel in corrosive environments, the literature had a gap concerning how this steel responds to the loads that bridge structures experience during their service lives. To investigate this and facilitate the future use of A1010 steel, this study devised a holistic structural testing program.</p> <p>A 52 ft 9 in. long girder was designed, fabricated, and tested (while subjected to four-point bending), with the results further compared to the current American Association of State Highway and Transportation Officials (AASHTO) Load and Resistance Factor Design (LRFD) Bridge Design Specifications. Additionally, tensile and fatigue tests were conducted to obtain the mechanical and fatigue behavior for A1010 steel. Furthermore, live load tests for the A1010 bridge were conducted to identify any changes in behavior that occurred with time. Also, data were analyzed for differences in response between the A1010 and A709 steel girders. The research resulted in the following conclusions from the laboratory and field results:</p> <ul style="list-style-type: none"> • The predictions obtained utilizing actual material properties were reasonable compared to the results obtained from the laboratory test, which indicates the A1010 girder's ability to meet AASHTO design requirements. • No apparent differences were observed between the A1010 and A709 girders during field testing. Additionally, for all load cases, the maximum measured distribution factors were less than those calculated using the AASHTO equations. • The live-load tests performed on the A1010 steel bridge over two years indicated that the changes in structural performance were minimal. <p>Long-term monitoring of an A1010 steel cross frame and a research panel will be carried out to provide essential information on galvanic corrosion throughout the serviceable lifetime of the bridge. The results will help in understanding the importance of controlling and reducing galvanic corrosion for future A1010 steel bridges in the region.</p>			
17. Key Words A1010 steel bridge—A1010 steel testing—LRFD specification comparisons—Salix Interchange Bridge—Woodbury County Bridge		18. Distribution Statement No restrictions.	
19. Security Classification (of this report) Unclassified.	20. Security Classification (of this page) Unclassified.	21. No. of Pages 93	22. Price NA

EVALUATION OF THE PERFORMANCE OF A1010 BRIDGE STEEL

**Final Report
January 2020**

Principal Investigator

Brent Phares, Research Associate Professor
Bridge Engineering Center, Iowa State University

Co-Principal Investigators

Travis Hosteng, Co-Director
National Center for Wood Transportation Structures, Iowa State University

Jay Shen, Associate Professor
Civil, Construction, and Environmental Engineering, Iowa State University

Research Assistant

Weizhuo Shi

Authors

Brent Phares, Behrouz Shafei, and Weizhuo Shi

Sponsored by
Iowa Department of Transportation

Preparation of this report was financed in part
through funds provided by the Iowa Department of Transportation
through its Research Management Agreement
with the Institute for Transportation
(InTrans Project 16-562)

A report from
Bridge Engineering Center
Iowa State University
2711 South Loop Drive, Suite 4700
Ames, IA 50010-8664
Phone: 515-294-8103 Fax: 515-294-0467
www.instrans.iastate.edu

TABLE OF CONTENTS

ACKNOWLEDGMENTS	xi
EXECUTIVE SUMMARY	xiii
CHAPTER 1. INTRODUCTION	1
1.1 Project Background.....	1
1.2 Research Objectives and Scope.....	2
1.3 Research Tasks.....	2
Task 1 – Literature Review	2
Task 2 – Laboratory Evaluation of A1010 Girders to Meet AASHTO Design Provisions	3
Task 3 – Testing of Galvanic Corrosion Potential	3
Task 4 – Testing of Fatigue Behavior	3
Task 5 – Bridge Field Testing	3
1.4 Report Layout.....	4
Literature Review (Chapter 2).....	4
Laboratory Testing (Chapters 3 and 4).....	4
Fatigue Investigation (Chapter 5).....	5
Field Testing (Chapter 6).....	5
Galvanic Corrosion Testing (Chapter 7)	5
Summary, Conclusions, and Recommendations(Chapter 8).....	5
CHAPTER 2. LITERATURE REVIEW	6
2.1 Corrosion Issues for Structural Steel Bridges	6
2.2 Weathering Steel Bridge Overview.....	7
2.3 ASTM A1010 Bridge Steel.....	9
2.3.1 Background and Projects	9
2.3.2 Material Properties	10
2.3.3 Weldability	12
2.3.4 Corrosion Resistance	12
2.3.5 Galvanic Corrosion.....	14
2.3.6 Fatigue Behavior.....	16
CHAPTER 3. LABORATORY TESTING	17
3.1 Introduction	17
3.2 Material Property of A1010 Steel	18

3.2 Specimen Design Details	20
3.3 Test Setup.....	22
3.3.1 Test A – 50% Yield Moment Testing for Plate Girder.....	22
3.3.2 Test B – Service Load Testing for Steel-Concrete Composite Section.....	23
3.3.3 Test C – Ultimate Load Testing for Steel-Concrete Composite Section.....	30
CHAPTER 4. LABORATORY TEST RESULTS	32
4.1 Results of Test A.....	32
4.2 Results of Test B	34
4.3 Results of Test C	37
4.4 Laboratory Test Summary and Conclusions	45
CHAPTER 5. FATIGUE TESTING.....	47
5.1 Introduction	47
5.2 Test Program	47
5.2.1 Specimen Preparation	47
5.2.2 Loading Protocols.....	49
5.3 Fatigue Testing Results	49
5.4 Conclusions and Recommendations.....	51
CHAPTER 6. FIELD TESTING OF THE WOODBURY COUNTY SALIX INTERCHANGE BRIDGE.....	52
6.1 Introduction	52
6.2 Bridge Description	52
6.3 Instrumentation Plan	54
6.4 Loading Plan	56
6.5 Load Test Results (2017)	58
6.5.1 Comparison in Behavior between the A1010 Steel and A709 Steel	59
6.5.2 Distribution Factors	60
6.6 Load Test Results (2018)	64
6.6.1 Comparison in Behavior between the A1010 Steel and A709 Steel	64
6.6.2 Distribution Factors	66
6.7 Comparison in Bridge Performance Occurring within Two Years.....	66
6.8 Field Test Summary and Conclusions.....	67
CHAPTER 7. GALVANIC CORROSION TESTING.....	68
7.1 Introduction	68

7.2 Cross Frame Monitoring	68
7.3 A1010 Plate Exposure Testing.....	71
7.4 Ongoing Corrosion Measurements.....	73
CHAPTER 8. SUMMARY, CONCLUSIONS, AND RECOMMENDATIONS	75
8.1 Summary	75
8.2 Conclusions	75
8.3 Future Work	76
8.4 Recommendations for Additional Future Research	76
REFERENCES	77

LIST OF FIGURES

Figure 1. Typical bridge condition as a function of time.....	6
Figure 2. Weathering steel bridge elements.....	8
Figure 3. Close-up of patina formation.....	9
Figure 4. Tensile strength distribution for A1010 steel.....	12
Figure 5. Comparison of reaction between weathering and stainless steel.....	13
Figure 6. Optical metallography of the base metal for A1010 steel.....	18
Figure 7. Tensile coupon sample preparation.....	19
Figure 8. Details of plate girder specimen.....	21
Figure 9. Loading setup for plate girder under 50% yield moment.....	22
Figure 10. Instrumentation plan for Test A.....	23
Figure 11. Geometrical dimensions and detailing of the composite beam section.....	24
Figure 12. A1010 composite beam fabrication.....	25
Figure 13. Loading setup for composite beam under 50% yield moment.....	27
Figure 14. Instrumentation plan for Test B.....	28
Figure 15. Instrumentation program.....	30
Figure 16. Instrumentation plan for Test C.....	31
Figure 17. Load vs. displacement, Test A.....	33
Figure 18. Strain profile under Test A (50 kips).....	33
Figure 19. Load vs. displacement, Test B.....	35
Figure 20. Strain profile under Test B (first time, 66 kips).....	36
Figure 21. Strain profile under Test B (second time, 66 kips).....	36
Figure 22. Plastic forces for A1010 composite section.....	38
Figure 23. Ultimate flexural performance for A1010 specimen.....	40
Figure 24. Maximum load-displacement curve, S2 (mid-span section).....	41
Figure 25. Maximum load-displacement curve, S1 and S3 (quarter-span sections).....	42
Figure 26. Load-longitudinal slip relationships, S0 and S2.....	43
Figure 27. Longitudinal strain distribution, S2.....	44
Figure 28. Strain distribution of under different load levels, S2.....	45
Figure 29. Hourglass shaped fatigue coupons.....	48
Figure 30. Specimens for A1010 fatigue testing.....	48
Figure 31. Fatigue testing setup.....	49
Figure 32. S-N curve for A1010 steel.....	50
Figure 33. Comparison between S-N curve of A1010 and other steels.....	51
Figure 34. Structural steel framing plan for Salix Bridge.....	53
Figure 35. Cross-section view of Salix Bridge superstructure.....	53
Figure 36. Salix Bridge.....	54
Figure 37. Plan view arrangement for instrumentation (east-end span).....	55
Figure 38. Cross-section view of strain gauge locations.....	55
Figure 39. Instrumentation setup.....	56
Figure 40. Iowa DOT Salix Bridge load testing truck.....	57
Figure 41. Configuration of loading truck and axle loads.....	57
Figure 42. Truckload paths for bridge testing.....	58
Figure 43. Response between A1010 and A709 under Load Case 1 and 5.....	59
Figure 44. Response of all girders under Load Case 3.....	60

Figure 45. Maximum strain response of all girders under each load case	62
Figure 46. Measured load distribution factors under each load case	63
Figure 47. Comparison of experimental and AASHTO-specified load distribution factors	64
Figure 48. Response between A1010 and A709 under Load Case 1 and 5	65
Figure 49. Response between all girders under Load Case 3	65
Figure 50. Measured load distribution factors under each load case	66
Figure 51. Comparison of distribution factors between 2017 and 2018	67
Figure 52. Concrete deck removal from A1010 composite beam	69
Figure 53. Cross frame setup for galvanized corrosion monitoring	70
Figure 54. A1010 plate mounting in the field (December 2017)	71
Figure 55. A1010 steel plate with stainless steel and galvanized steel bolts and welded connection	72

LIST OF TABLES

Table 1. Specified composition of A1010 steel (wt. %)	10
Table 2. Specified mechanical properties of A1010, A709, and A240 steel	11
Table 3. Compositions of different types of steel and A1010 corrosion indices (CIs)	13
Table 4. Summary of A1010 coupon tensile test	20
Table 5. Compression test results for concrete deck	24
Table 6. Comparison of the strain results under Test A (50 kips)	34
Table 7. Comparison of the strain results under Test B (50 kips)	37
Table 8. Comparisons between ultimate flexural strength	39
Table 9. Dimensions of A1010 specimens and standard recommendations	48
Table 10. Number of cycles to fracture for A1010 specimens	50
Table 11. Loading scenarios	58
Table 12. Calculated load distribution factors (2017)	63
Table 13. Calculated load distribution factors (2018)	66
Table 14. Weight measurements for A1010 panel	72
Table 15. Thickness measurements for A1010 plate	73

ACKNOWLEDGMENTS

The authors would like to acknowledge the Iowa Department of Transportation for sponsoring this work. They also would like to thank the technical advisory committee for their guidance on this project.

Finally, the authors would like to thank Doug Wood, Travis Hosteng, Katelyn Freeseaman, and Owen Steffens with the Bridge Engineering Center and the Structural Engineering Research Laboratory at Iowa State University for their assistance in conducting various aspects of the laboratory and field evaluation.

EXECUTIVE SUMMARY

In 2016, the Iowa Department of Transportation (DOT) replaced a bridge in Woodbury County (on County Road K25 over I-29) with a four-span bridge partially constructed using ASTM A1010 bridge steel. The general goals of this project were to evaluate the fundamental behavior of girders fabricated using A1010 steel, evaluate the potential for galvanic corrosion when various fastener types are used, and assess the in situ performance of the bridge.

Despite the wealth of information on the durability of A1010 steel in corrosive environments, the literature had a gap concerning how this type of steel responds to the loads that bridge structures experience during their service lives. Therefore, a comprehensive experimental program was carried out to investigate the performance of A1010 steel under a four-point bending scenario to determine the plate girder and composite flexural behavior.

A 52 ft 9 in. long girder was designed, fabricated, and tested, with the results also compared to the current American Association of State Highway and Transportation Officials (AASHTO) Load and Resistance Factor Design (LRFD) Bridge Design Specifications. Additionally, tensile and fatigue tests were conducted to obtain the mechanical and fatigue behavior for the A1010 steel. Furthermore, live load tests for the A1010 steel bridge were conducted to identify any changes in behavior that occurred with time. Also, the data were analyzed for differences in response between the A1010 and A709 steel girders.

From the work carried out in this study, the researchers came to the following conclusions:

- The predictions obtained utilizing actual material properties were reasonable compared to the results obtained from the laboratory testing, which indicates the A1010 girder's ability to meet the AASHTO design requirements. When the designed material properties were utilized for hand calculations, the flexural capacity measured from the laboratory test was 15.4% higher. This may be due to the difference between the material properties of A1010 steel obtained from tensile tests and the recommendation in design.
- The fatigue limit for A1010 steel was found to be between 37.4 ksi and 40.8 ksi in the laboratory testing. Thus, A1010 steel can provide adequate fatigue resistance according to current fatigue design provisions.
- In general, no apparent differences were observed between the A1010 and A709 girders during field testing. Additionally, the calculated distribution factors from the measured field strains and the AASHTO-recommended equations were investigated for comparison. For all cases, the maximum measured distribution factors were less than those calculated using the equations.
- The live load tests performed on the A1010 steel bridge over two years indicated that the changes of structural performance were minimal.

Further field studies are being conducted to evaluate the potential for galvanic corrosion when different types of bolts and welds are used. To achieve this goal, the following work will be carried out:

- Long-term observational monitoring of galvanic corrosion of a full-scale cross frame will be conducted, which will provide data for two types of bolted connections, i.e., stainless steel bolts and galvanized steel bolts.
- Long-term monitoring of an A1010 plate placed at the bridge site will be conducted and periodically documented for the development of corrosion products. The data and analysis will be presented in a future report, which will assess the galvanic behavior for the A1010 steel panel throughout the exposure time.

The results of this work will help in understanding the importance of controlling and reducing galvanic corrosion for future A1010 steel bridges located in the region.

CHAPTER 1. INTRODUCTION

1.1 Project Background

Corrosion, known as the deterioration of a metal as a result of chemical reactions between it and the atmospheric conditions, can significantly jeopardize the long-term performance and integrity of a steel bridge. Each year, about \$273 billion is funded for corrosion maintenance in the US, and \$8.3 billion of that is spent on repair and replacement of highway bridges (Koch et al. 2002, Cambier 2014).

Many factors affect the extent of corrosion, such as temperature, humidity, salinity, and type of metal. However, while these environmental stressors are unavoidable, innovative material selection, such as choosing a corrosion-resistant structural steel, can avoid damage or an unacceptable appearance due to corrosion products and can achieve a longer service life for bridges.

Steel highway bridges are susceptible to corrosion over time. Thus, the cost of their maintenance, such as painting or replacing, is expected to increase. The maintenance costs will be magnified with the indirect costs associated with possible bridge closures and the loss of business.

Painted conventional steel and unpainted ASTM A709 50W weathering steel have been used traditionally as mitigation for corrosion. However, bridges with these steels or treatment may require regular and costly maintenance over their design lives, when the protective oxide or oxyhydroxide layer is barely formed, for example, for A709 weathering steel—due to the lack of the frequent drying required (FHWA 2011).

One structural stainless steel, which is described in ASTM A1010 (2014), has been recently utilized by some departments of transportation (DOTs) in the US to overcome the corrosion issues of conventional weathering steel in bridge construction (Via and Harrop 2017, Seradj 2015). A1010 steel is relatively new to the market of structural stainless steel and is a nominal 12% chromium (10.5% minimum and 12.5% maximum) steel that is reported to have enhanced corrosion resistance compared to traditional painted structural steels, weathering steels, and galvanized steels. A1010 steel has been successfully used in environmentally aggressive applications, such as coal rail cars and coal processing equipment. Although more expensive initially, it is possible that bridges constructed using A1010 may have longer service lives and, therefore, lower overall life-cycle costs.

In 2016, the Iowa DOT replaced a bridge in Woodbury County, on County Road (CR) K25 over I-29, with a four-span bridge partially constructed using ASTM A1010 bridge steel. Despite the wealth of information on the durability of A1010 steel in corrosive environments, the literature had a gap concerning how this type of steel responds to the loads that bridge structures experience during their service lives. To investigate this critical aspect and facilitate the future use of A1010 steel, this study devised a holistic structural testing program.

A 52 ft 9 in. (16 m) long girder was designed, fabricated, and tested under a four-point bending setup. The girder's ability to meet the design expectations was assessed by comparing the results with the American Association of State Highway and Transportation Officials (AASHTO) Load and Resistance Factor Design (LRFD) Bridge Design Specifications (AASHTO 2017). In addition, tensile and fatigue tests were carried out to obtain an in-depth understanding of the performance of A1010 steel under both monotonic and cyclic loading scenarios. This led to the development of load-displacement, stress-strain, and S-N curves that can be further employed for a safe and efficient design of structural members made with A1010 steel. Moreover, field testing over two years following the construction of the Woodbury County bridge was performed to assess the in situ performance of A1010 steel girders.

1.2 Research Objectives and Scope

A1010 steel is relatively new to the market of structural stainless steel and seldom has been utilized for bridge construction in the US. Although the development of A1010 steel in the US is very recent, it is rapidly gaining interest for application in highway bridges. Valuable research studies on A1010 steel coupons have been conducted to investigate the chemical and mechanical properties, weldability, constructively, cost, and general uniform corrosion properties under accelerated conditions (ArcelorMittal 2010, 2013, and 2015, Cook and Granata 2002, Fletcher 2011, Fletcher et al. 2003 and 2005, Fletcher and Gagnepain 2007, Groshek 2017, Seradj 2010 and 2015, Via and Harrop 2017). However, limited efforts have focused on the evaluation of the structural performance and fatigue behavior of A1010 steel, or the service condition of corresponding bridges made with A1010 steel in the field.

The primary goals of this work were to evaluate the fundamental structural behavior of girders fabricated using A1010 steel and to characterize their fatigue behavior. Thus, a full-scale experimental program was established, and the results were compared to predictions obtained from AASHTO equations. Also, fatigue testing was performed with the goal of investigating fatigue characteristics using the method of fatigue life prediction, with the performance compared to that of conventional steel girders.

1.3 Research Tasks

The following tasks were established for this work:

Task 1 – Literature Review

A literature review was conducted to identify pertinent information related to the use of ASTM A1010 steel. This literature review included identifying ongoing and completed research related to the corrosion resistance, mechanical properties, and structural performance of A1010 steel. Also, information on actual installations was sought and summarized from state DOTs that have used A1010 steel on bridges.

Task 2 – Laboratory Evaluation of A1010 Girders to Meet AASHTO Design Provisions

With any new material, there are questions about how a structure designed with the material will meet current design assumptions and provisions. In many ways, testing of this type is needed merely to convince people that “it will work.” The goal of Task 2 was to complete such testing.

For this testing, a 52 ft 9 in. long girder was fabricated as part of a Woodbury County bridge project and delivered to the Structural Engineering Research Laboratory at Iowa State University. The girder exactly replicated what had been constructed and used as two of the four girders in the Woodbury County bridge.

To test the girder’s ability to meet current AASHTO design provisions, a composite concrete deck was constructed on top of the girder, and the composite section was tested under four-point bending. Among other items, this testing was to ensure that the section had adequate ductility.

Task 3 – Testing of Galvanic Corrosion Potential

Following the completion of the testing in Task 2, two approximately 12 ft long sections of the girder were removed and retained to test their galvanic corrosion potential when used with two different types of bolts. The two sections of the steel beam were connected with a galvanized steel cross frame. At one beam location, the girder and cross frame were connected using stainless steel bolts, and, on the other side, galvanized steel bolts were used. The entire system was placed outside and observed for the length of the project to monitor the development of corrosion.

Additionally, an A1010 corrosion monitoring plate was placed at the bridge site, and the research team periodically monitored it and documented the development of corrosion products.

Task 4 – Testing of Fatigue Behavior

Coupon testing and its associated mathematical model were developed to predict the fatigue life of A1010 steel. In this study, the stress-life method was adopted to predict the fatigue life for A1010 steel. In the stress-life method, the calculated elastic stress range was used with an S-N curve (a log-log plot of stress range versus the number of cycles to failure) to determine the fatigue life.

Task 5 – Bridge Field Testing

Following construction, the bridge was live-load tested. For field testing, a variety of strain transducers were installed on the bridge superstructure. These gauges were placed on both the A1010 girders and the A709 girders and components.

A loaded truck of known weight and dimensions was driven across the bridge with the resulting response data collected. About a year later, the test was repeated with similar data collected. The data from both tests were compared to identify any changes in behavior that occurred with time. Additionally, the data were analyzed for differences in response between the two steel types used for the bridge girders.

1.4 Report Layout

This final report consists of seven additional chapters and a References section.

Literature Review (Chapter 2)

This chapter includes the results of a literature search and review and summarizes current knowledge, including substantive findings, as well as theoretical and practical contributions related to ASTM A1010 steel.

Laboratory Testing (Chapters 3 and 4)

Chapters 3 and 4 cover the laboratory tests performed on an A1010 steel girder and the results.

- Test A – 50% yield moment testing for the A1010 plate girder

To examine the flexural performance of the A1010 plate girder and verify the loading system, a two-point bending test was performed on the girder. To minimize the possibilities of damaging the girder, testing was limited to inducing moments in the girder to only 50% of the yield moment for the plate girder. The data that were recorded were also compared to the results obtained from hand calculations.

- Test B – 50% yield moment testing for the A1010 steel-concrete composite section

To investigate the flexural performance of the A1010 steel-concrete composite section and verify the loading system, a two-point bending test was performed again on the A1010 plate girder with the concrete deck that had been placed over it. To minimize the possibilities of damaging the girder during this testing, testing was limited to inducing moments in the girder to only 50% of yield for the steel-concrete composite section.

- Test C – Ultimate capacity for the A1010 steel-concrete composite section

To evaluate the ultimate flexural capacity of the composite girder, the A1010 steel-concrete composite section was tested under two-point bending until failure. The measured results were compared to the hand calculations obtained from the AASHTO equations.

Fatigue Investigation (Chapter 5)

This chapter covers the testing to evaluate the fatigue behavior for A1010 steel. Coupon testing and its associated mathematical model were developed to predict the fatigue life of A1010 steel.

Field Testing (Chapter 6)

This chapter covers the field testing conducted after bridge construction and one and two years later.

Galvanic Corrosion Testing (Chapter 7)

This chapter covers the galvanic corrosion testing, which will be ongoing, that evaluated two specimens: a full-scale A1010 steel cross frame and an exposed A1010 research plate.

Summary, Conclusions, and Recommendations(Chapter 8)

In this chapter, the fundamental conclusions of this project are summarized based on all aspects of the work, planned future work is described, and recommendations for additional future work are listed.

CHAPTER 2. LITERATURE REVIEW

A literature review of technical publications was conducted to identify pertinent information related to using ASTM A1010 steel. This literature review included identifying ongoing and completed research for A1010 steel related to its physical properties, mechanical properties, structural behavior, corrosion performance, and cost analysis. Also, information on actual installations was sought and summarized from state DOTs that have used A1010 steel in bridges.

2.1 Corrosion Issues for Structural Steel Bridges

According to a report submitted to Congress from the Federal Highway Administration (FHWA), in 2012, there were 607,380 bridges in the US, with 30% of them categorized as structurally deficient or functionally obsolete (FHWA 2016). Almost 4 in 10 of these bridges were 50 years old or older, which indicated that most of these bridges are in the process of increasing maintenance costs and in need of repairs or replacement.

Steel highway bridges, which accounted for 200,000 of the total number of bridges, have a high potential to corrode with time. Correspondingly, the cost for the further required maintenance work on them, such as painting or replacement, will increase. Figure 1 shows the relationship between the cost of maintenance for a typical bridge and its structural condition from a white paper published by NACE International (2012).

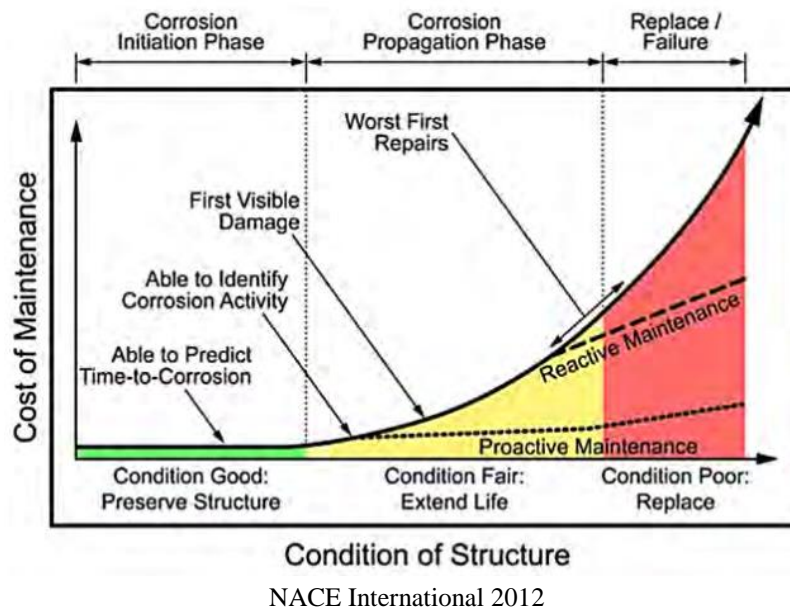


Figure 1. Typical bridge condition as a function of time

As shown, not only does the price of maintenance tend to increase with the deteriorating condition of the structure, but the rate of the cost also increases exponentially with the worsening condition of the structure. This implies that, for a maintenance cost on a bridge in the corrosion

propagation phase that is not addressed this year, the cost may increase exponentially in the next year, and costs will continue to grow until the bridge needs to be replaced.

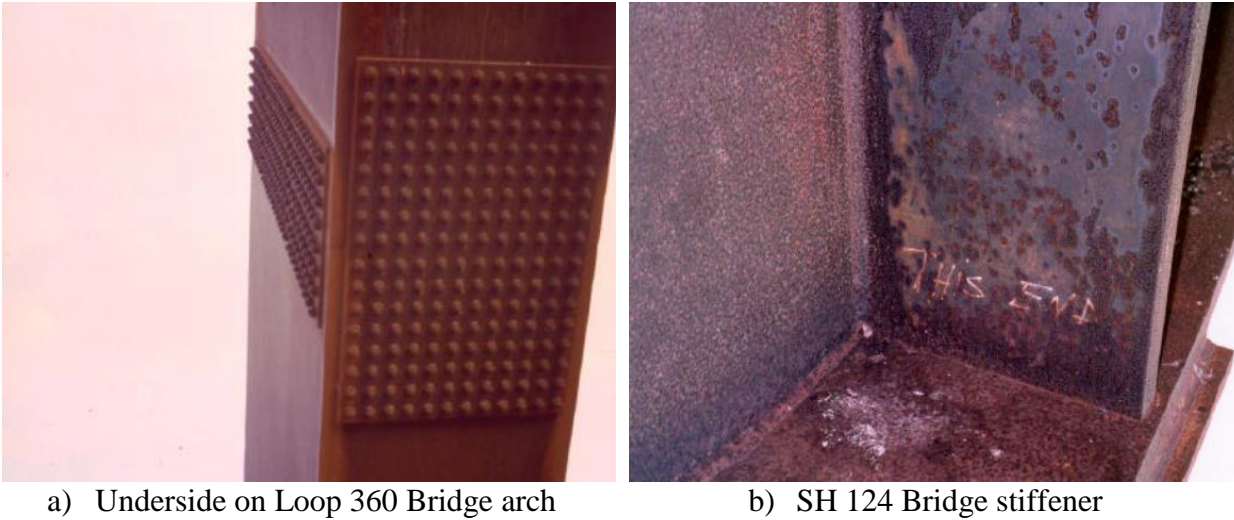
2.2 Weathering Steel Bridge Overview

ASTM A588 and A709 steel are characterized as weathering steels that have been utilized for bridge infrastructures to mitigate their corrosion damage in the US (ASTM 2015a, 2017). The first weathering steel bridge was constructed in Moline, Illinois, and opened in 1964. Since then, the use of weathering steel has spread nationwide for bridge infrastructure because of its robust performance and improved atmospheric corrosion resistance with its potential to form passive, protective rust or patina on the surface (Kihira et al.1990).

However, the protective patina is not guaranteed to form on weathering steel in severe service conditions, such as coastal and deicing salt environments (Albrecht and Naeemi 1984, Cook et al. 1998, Crampton et al. 2013, Fletcher 2005 and 2011, Fletcher et al. 2003 and 2005, McDad et al. 2000). In 1982, 49 bridges in Illinois, Maryland, Michigan, New York, New Jersey (Turnpike), North Carolina, and Wisconsin, were inspected by a group from the American Iron and Steel Institute (AISI) (1984) with the goal of evaluating the corrosion resistance performance of weathering steel. Most of the inspected bridges showed decent corrosion resistance performance, but five bridges exhibited heavy corrosion due to the inadequate formation of a protective patina. Salt contamination and prolonged time of wetness were concluded to be the two main reasons to account for the difficulties in the creation of patina.

To investigate the protective layer formation mechanism for weathering steel after long-term atmospheric exposure, Cook et al. (1998) conducted a study utilizing a series of techniques (Mössbauer spectroscopy, Raman spectrometry, and x-ray diffraction). The researchers studied the protective layers that formed between 11 and 29 years after construction on exposed weathering steel coupons in industrial environments in the US and Japan. The researchers found that a protective layer of nanophase goethite formed at the steel surface to inhibit further corrosion damage. However, they also concluded that the requirement of frequent drying and the presence of chlorides in coastal and deicing salt environments were undesirable for the formation of such a protective patina for weathering steels.

McDad et al. (2000) presented the issue associated with patina formation in a survey conducted for the Texas DOT (TxDOT) and Cook and Granata (2002) did so in a survey for the New York State DOT (NYSDOT). The protective oxide film was found to be not well developed for some weathering steel bridges in areas that were not directly exposed to wet-dry cycles. Figure 2a shows an example at a girder splice section where the top and sides of the steel developed a well and adhered protective film.



McDad et al. 2000

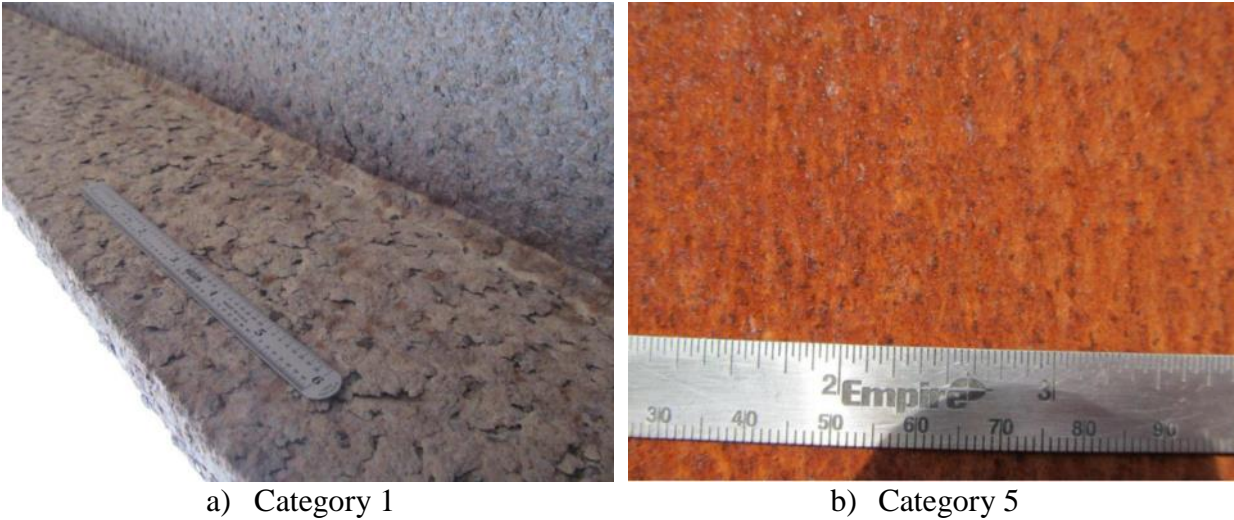
Figure 2. Weathering steel bridge elements

However, when the steel is not directly exposed to rain and sun on the bottom surface, the patina is not well formed. Figure 2b shows an example of limited patina forming on a weathering steel surface on the SH 124 Bridge where the mill steel was observed in some areas, which resulted from the high chloride environment of the Gulf Intracoastal Waterway.

Cook and Granata (2002), conducted a statewide site survey for the NYSDOT to assess the performance of patina formations for weathering steel bridges. They reported there were about 50 bridges inspected along the I-390 corridor in the Rochester, New York, vicinity for which the protective rust layer did not develop.

Crampton et al. (2013) inspected 31 bridges in Iowa to document the quality of patina formation for weathering steel bridges. These bridges were categorized into 12 groups based on the various location environments. A series of testing methods were utilized to rate these bridges, including visual inspection, tape adhesion testing, chloride testing, color testing, laboratory analysis of corrosion product of physical samples, and high-pressure washing. In the field visual inspection, bridges were rated from Category 1, indicating a substantial failure of patina, to Category 5, indicating an excellent protective behavior with an immature, developing patina, to represent different stages of performance. Crampton et al. 2013

Figure 3 illustrates the comparison between a heavily chalked surface due to unformed patina and a typical well-adhered patina for weathering steel girder bridges.



Crampton et al. 2013

Figure 3. Close-up of patina formation

As shown, the delamination of the patina on the surface of weathering steel, which may permit salt and moisture to penetrate the rust interlaminations, may induce additional corrosion damage.

Therefore, weathering steel bridges cannot be guaranteed to eliminate maintenance for corrosion in severe service environments where the protective rust film is not able to form on the surfaces. In circumstances where the performance of weathering steel is unsatisfactory, innovative material selection, such as choosing a corrosion-resistant structural steel, can avoid damage or an unacceptable appearance and can achieve a longer service life.

2.3 ASTM A1010 Bridge Steel

2.3.1 Background and Projects

To eliminate regular and costly maintenance over the design life of bridges, a fairly new type of structural steel, ASTM A1010 steel, has been utilized by some DOTs in the US (Via and Harrop 2017, Seradj 2015, Fletcher et al. 2003, Fletcher and Gagnepain 2007, ArcelorMittal 2015). A1010 steel is relatively new to the market of structural stainless steel and is a nominal 12% chromium (10.5% minimum, 12.5% maximum) material that is reported to have enhanced corrosion resistance over that of traditional painted structural steel, weathering steel, and galvanized steel. When this report was written, only six A1010 steel bridges had been built in the US.

In 2004, a short-span, box-girder bridge was built using A1010 steel on Fairview Road over the Glenn-Colusa Main Canal near Williams in Colusa County, California (Fletcher and Gagnepain 2007). This bridge is a multi-cell girder bridge 72 ft 6 in. long and 31 ft 6 in. wide. Finite element modeling was conducted to estimate loads and deflections. Shortly after the bridge was opened to the traffic, the deflections and stresses were measured from the strain gauges installed

in various locations on the bridge. The obtained stresses and deflections were in good agreement with the design assumptions.

The second A1010 bridge was built over a local creek at a Coatesville, Pennsylvania, steel plant in 2012 (ArcelorMittal 2013).

The Oregon DOT constructed two A1010 steel bridges spanning more than 120 ft (one in 2012 and the other in 2013). The first was built near Astoria at Dodge Creek, and the other one was located on US 30 at Mill Creek.

In 2016, the US 340 bridge was constructed in Waynesboro, Virginia, with ASTM A1010 steel plate girders, cross frames, and stainless-steel bolts. This bridge was built because of corrosion concerns associated with the low clearance above the average water level (8.5 ft), the high potential of being inundated after storms, and the close location to an industrial area. The stainless-steel fasteners were utilized for bolted girder splices to ensure the corrosion-resistance performance was similar to that of the primary A1010 steel girders.

In 2016, the Iowa DOT built a four-span bridge in Woodbury County using both ASTM A1010 steel and ASTM A709 weathering steel. This bridge is a two-lane, four-span, continuous, steel girder bridge located on CR K25 over I-29 (called the Salix, Iowa, interchange). As the replacement of the previous precast, prestressed concrete beam bridge, this bridge was skewed at 17 degrees with a total length of 403 ft and a width of 40 ft.

2.3.2 Material Properties

There have been numerous studies to investigate the material properties for A1010 steel (ArcelorMittal 2015, Daghash and Ozbulut 2017, Fletcher 2011, and Fletcher and Gagnepain 2007). Table 1 lists the specified chemical composition of A1010 steel from the ASTM standard (2014) and the steel producer, ArcelorMittal USA.

Table 1. Specified composition of A1010 steel (wt. %)

	C	Mn	P	S	Si	Cr	Ni	N	Mo
ASTM A1010	0.030	1.50	0.040	0.010	1.00	10.5-12.5	1.50	0.030	-
ArcelorMittal	0.025	1.50	0.040	0.010	0.70	11.0-12.5	1.00	0.030	0.20-0.35

As a corrosion-resistant metallic alloy, A1010 steel is a low-cost 12%-chromium dual-phase stainless steel, first developed by ArcelorMittal USA. The required mechanical properties of A1010 steel, A709 weathering steel, and A240 stainless steel are documented by ASTM International specifications as shown in Table 2.

Table 2. Specified mechanical properties of A1010, A709, and A240 steel

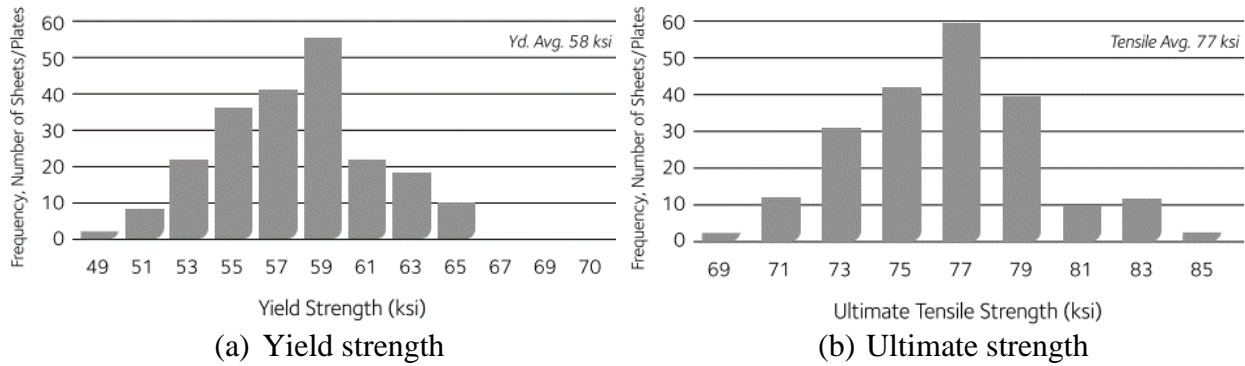
ASTM Grade	Yield strength, min, ksi [MPa]	Tensile strength, min, ksi [MPa]	Elongation in 2 in. (50 mm), min, %	Brinell hardness, max.
A1010 Grade 40	40 [275]	66 [455]	18	Not required
A1010 Grade 50	50 [345]	70 [485]	18	Not required
A709 Grade 50W	50 [345]	70 [485]	21	–
A240	40 [275]	66 [455]	18	–

Sources: ASTM 2014, 2017, and 2018

Based on the data in the table, A1010 is confirmed to have a minimum yield strength of 50 ksi (275 MPa) that is equivalent to A709 Grade 50W. ArcelorMittal (2015) has conducted tensile testing for measuring the yield strength and ultimate tensile strength of A1010 steel on more than 200 coupons. It was concluded that the average for yield strength was 58 ksi (400 MPa) and ultimate strength was 77 ksi (531 MPa).

Daghash and Ozbulut (2017) conducted a study to investigate the tensile strength for specimens with different thicknesses oriented parallel and transverse to the rolling direction. The researchers found that, for specimens cut parallel to the rolling direction, the average yield stress and ultimate strength can increase by increasing the thickness. However, for specimens oriented transverse to the rolling direction, the results showed higher strength compared to the ones oriented parallel to the rolling direction.

The Charpy V-notch (CVN) test can determine the fracture toughness for steel materials. Fracture toughness is the ability of a steel material to absorb the energy and plastically deform while breaking when subjected to an impact load. ArcelorMittal (2015) performed a series of CVN impact tests on more than 100 specimens for A1010 steel subjected to variations of temperature between -50°F (-45°C) to 200°F (93°C). The results confirmed that A1010 steel could meet the CVN requirements for high-performance steel Grade HPS 50W, as shown in Figure 4.



ArcelorMittal 2015

Figure 4. Tensile strength distribution for A1010 steel

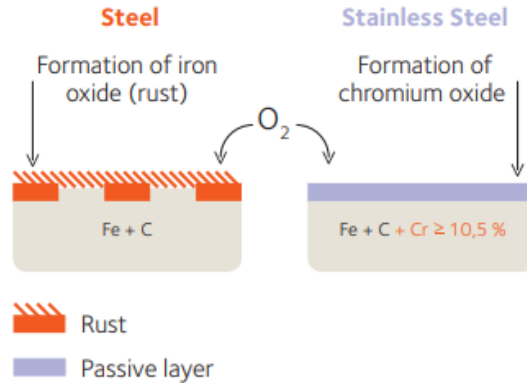
2.3.3 Weldability

Since A1010 steel is relatively new to the market, it is not currently included in the AASHTO and American Welding Society (AWS) D1.5 Bridge Welding Code. Seradj (2010) conducted a study to evaluate the weldability of A1010 steel using all processes that are currently employed for bridge fabrication. In his study, four 1 in. (2.54 cm) long sample sections were cut from four A1010 T-welded samples that were made by utilizing an automatic submerged arc and semi-automatic flux core welding process. All of these samples could meet the AASHTO LRFD Design Specifications, and all of them failed in the weld, with the fracture path through the weld metal.

To obtain the fatigue behavior, Lijas and Ericsson (2002) conducted high-cycle fatigue testing focused on UNS S32205 duplex stainless steel and their welds and compared the results with austenitic stainless steel and carbon steel. The researchers concluded that the welds had a limited effect on the fatigue strength for all steels. Even though the tested austenitic steel had higher tensile strength than duplex steel, lower fatigue strength was obtained for austenitic steel. Among all the steels, duplex steels showed a prominent fatigue behavior, which was more than twice the fatigue strength of the carbon steel.

2.3.4 Corrosion Resistance

ArcelorMittal illustrates the difference between the mechanism of protective layer formation for weathering steel and stainless steel when in contact with moisture in the air (ArcelorMittal 2010) (see Figure 5).



ArcelorMittal 2010

Figure 5. Comparison of reaction between weathering and stainless steel

As shown in the figure, due to the contribution of chromium, instead of the formation of iron oxide (patina), a chromium oxide layer can be formed on the surface of the structural stainless steel, which will further protect the material from corrosion.

The atmospheric corrosion resistance performance can actually be determined from the weight percentage of each chemical composition of steel using the following Legault-Leckie equation (ASTM 2015b):

$$I = 26.01(\%Cu) + 3.88(\%Ni) + 1.20(\%Cr) + 1.49(\%Si) + 17.28(\%P) - 7.28(\%Cu)(\%Ni) - 9.10(\%Ni)(\%P) - 33.39(\%Cu)^2 \quad (1)$$

The larger index predicted from equation (1) indicates the better atmospheric corrosion resistance. Based on the chemical composition, the weathering corrosion index was comprehensively included for some structural steels summarized in Fletcher et al.'s study (2003), as shown in Table 3.

Table 3. Compositions of different types of steel and A1010 corrosion indices (CIs)

Steel	C	Mn	P	S	Si	Cu	Ni	Cr	Mo	V	Al	CI
A36	0.16	1.01	0.012	0.013	0.22	0.02	0.02	0.03	0.00	0.003	0.051	1.15
50W	0.10	1.18	0.012	0.011	0.36	0.30	0.31	0.53	0.01	0.039	0.048	6.62
70W	0.09	1.20	0.006	0.002	0.36	0.33	0.33	0.53	0.06	0.062	0.014	6.64
A1010	0.01	1.31	0.017	0.003	0.56	0.02	0.50	11.9	0.28	–	0.001	17.70

50W and 70W represent A709 weathering steel at the respective grades

As shown in the table, ASTM A36 carbon structural steel (ASTM 2019) has minimum atmospheric corrosion resistance. The corrosion index of ASTM A709 70W steel is 6.64, which is close to that of ASTM A709 50W steel (with 6.62). However, the atmospheric corrosion index of ASTM A1010 steel has the highest calculated value (of 17.70), and thereby has the most promising weathering performance.

Many laboratory accelerated cyclic corrosion tests and in situ exposure corrosion tests have been conducted to investigate the performance of corrosion resistance for A1010 steel (ArcelorMittal 2010 and 2015, Cook and Granata 2002, Fletcher 2011, Fletcher and Gagnepain 2007, Groshek 2017, Seradj 2015).

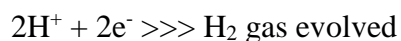
Fletcher (2011) established a study to evaluate the corrosion performance for A1010 steel and compare it to other bridge steel, such as ASTM A36 carbon structural steel and ASTM A588 weathering steel. The SAE J2334 laboratory corrosion test was performed through an automated cyclic corrosion chamber. This test protocol ensured the corrosion that formed was subjected to a high time-of-wetness and the presence of chlorides. A total of 100 cycles of NaCl solution was sprayed on the sets of three corrosion coupons for each type of steel. Two of the coupons were tested for mass loss, while x-ray diffraction (XRD) was utilized on the third coupon to characterize the formation of oxyhydroxides on the steel surfaces. The results revealed that, as the chromium content of the steel decreased from 11% to 5%, the corrosion resistance was reduced. All of the chromium steel showed a lower corrosion rate than that of the ASTM A588 steel. Also, the analyses of the corrosion on the cyclic corrosion coupons from the XRD results showed 11% chromium plates of steel had better corrosion rates than other steels.

To better understand the thickness loss in a severe corrosion environment for steel bridges, Cook and Granata (2002) and Fletcher and Gagnepain (2007) conducted field exposure tests on the Moore Drive Bridge in Rochester, New York. The first test was conducted in 2002 to investigate the field performance for ASTM A1010 and ASTM A588 steel, and the second one was followed by Fletcher and Gagnepain to evaluate the difference among different A1010 steels that contained 9% chromium steel (9Cr), 7% chromium and 2% silicon steel (7Cr2Si), and 7% chromium and 2% aluminum steel (7Cr2Al). The researchers concluded from the exposure tests that ASTM A1010 steel had the best performance in corrosion resistance concerning thickness loss of 0.58 mpy, while the thickness loss of ASTM HPS 50W was 2.03 mpy and ASTM A588 was 2.43 mpy. Also, the corrosion rate for 9Cr, 7Cr2Si, and 7Cr2Al was almost the same, which was supported by the thickness loss of 1.07, 1.20, and 1.11 mpy, respectively.

2.3.5 Galvanic Corrosion

Despite promising atmospheric corrosion resistance performance, one of the greatest corrosion concerns for utilizing A1010 steel in bridge applications is the potential for galvanic corrosion or bimetallic corrosion. Galvanic corrosion is an electrochemical process between two dissimilar metals when they are in electrical contact with each other. When galvanic corrosion takes place, polarization is induced by the formation of electrochemical cells at the anode and the cathode (Francis 2000).

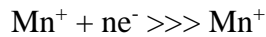
Two reactions could be defined in this electrochemical cell: anodic and cathodic, where each reaction is named a half-cell reaction. In the cathodic reaction, electrons provided by the anode metal move toward the cathode. In an acidic solution, the reaction is as follows:



In a neutral solution, the reaction is as follows:



In an anodic reaction, the electrons tend to be lost and oxidized. The reaction is generally written as follows:



where,

M represents a metallic element herein

e- is an electron

n is the valence of the metal as an ion

For A1010 steel bridges, high-strength bolts and associated nuts and washers are used in the connections, which introduces a high potential for galvanic corrosion. Groshek (2017) conducted a laboratory test to investigate the galvanic corrosion behavior for A1010 steel. Three investigations were conducted through cyclic salt spray testing: the galvanic corrosion of A1010 steel connected to plates and fasteners composed of dissimilar metals, the crevice corrosion of A1010 plates connected to other A1010 plates, and the effect of different surface preparation techniques on the corrosion behavior of A1010 steel. One cycle of the corrosion tests lasted for 20 hours and was divided into three stages: humid, salt solution application, and dry stage, and 80 cycles were carried out. Several methods of measurement—mass loss measurement, coating thickness measurement, and visual observations captured through photographs—were used to quantify the corrosion behavior for A1010 steel. These were the conclusions from the results:

- **A1010 steel plate:** Orientation of the specimen had a significant impact on thickness loss during the corrosion test. Horizontally oriented A1010 was found to be approximately 4 times more corrosion resistant than weathering steel, and 10 times more when vertically oriented. Use of steel shot blasting appeared to result in reducing thickness loss rates for A1010 plates compared to grit blasting, but may result in a more uneven formation of corrosion at earlier exposure to the environment. However, grit blasting was recommended for uniform aesthetic corrosion.
- **Assembled with other steel:** The bimetallic connections of carbon and weathering steels with A1010 steel were found to result in minor galvanic corrosion.. Hot-dip galvanized steel appeared to have a potential issue of galvanic corrosion with A1010 steel, and the shedding of the zinc coating caused staining on the A1010 surface.
- **Assembled with fasteners:** Galvanic corrosion was found to increase when a B6 stainless-steel bolt was connected with A1010 steel. However, the connection of A1010 steel and B8 Class 2 stainless-steel bolt assemblies exhibited negligible corrosion.

Recommendations on the following were also provided from this study: in situ corrosion tests of the A1010 plate (plate specimen and the existing bridge), galvanic corrosion of A1010 welding, stress corrosion cracking of A1010 plates, and performance of coatings applied to A1010 stainless steel.

Ebrahimi et al. (2018) developed a study to evaluate the galvanic coupling corrosion risk between A1010 steel and galvanized ASTM A325 Type I bolts, as well as that between A1010 steel and ASTM A320 B8 class 2 and A193 B6 stainless-steel bolts, and further compared the results to that with A588 weathering steels. The experiments were performed by measuring the galvanic coupling current and potential for the samples in the electrochemical cells, and visually inspecting the samples in the salt spray chamber. The researchers found that the galvanic corrosion potential between A1010 steel and B8 bolts was negligible given the measured corrosion current was minimal. However, the use of A325 galvanized bolts was not recommended in A1010 steel bridges due to the heavy corrosion that was obtained.

2.3.6 Fatigue Behavior

One of the most frequent causes of failure in structural steel bridges is fatigue. The stress concentrations at the corrosion spots or in the vicinity of the bolt connections or welds are the areas of most concern for fatigue issues. Unfortunately, no study to date has investigated the fatigue behavior for A1010 steel.

CHAPTER 3. LABORATORY TESTING

This chapter provides an in-depth description of the experimental testing methods utilized in this project.

3.1 Introduction

This chapter includes the laboratory testing program developed in this study for the evaluation of A1010 steel girders to meet AASHTO design provisions. With any new material, there are questions about how a structure designed with the material will meet current design assumptions and provisions. In many ways, testing of this type is needed to confirm that “it will work.”

For these laboratory tests, a 52 ft 9 in. long girder was fabricated as part of the Woodbury bridge project and delivered to the Structural Engineering Research Laboratory at Iowa State University. The girder section accurately replicated what was constructed in Woodbury County. To test the girder’s ability to meet current AASHTO design provisions, the following three tests were performed.

- **Test A – 50% yield moment testing for A1010 plate girder**

To examine the flexural performance of the A1010 plate girder and verify the loading system, the girder was subjected to a two-point bending test. To minimize the possibilities of damaging the girder, testing was carried out to limit the moments in the girder with it subjected to only 50% of the yield moment.

- **Test B – 50% yield moment testing for A1010 steel-concrete composite section**

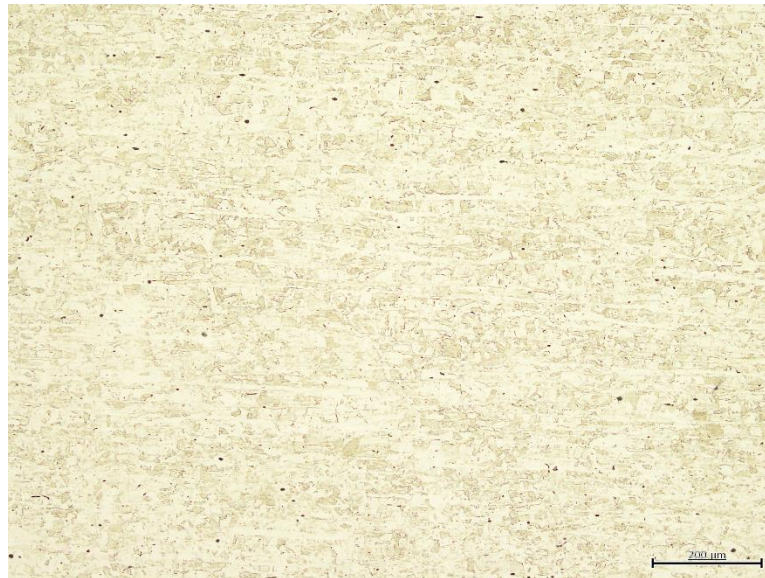
To investigate the flexural performance of the A1010 steel-concrete composite section and verify the loading system, the A1010 plate girder was subjected to a two-point bending test again with a concrete deck placed over it. To minimize the possibilities of damaging the girder, testing was limited to inducing moments in the girder with it subjected to only 50% of the yield moment for the steel-concrete composite section.

- **Test C – Ultimate capacity for an A1010 steel-concrete composite section**

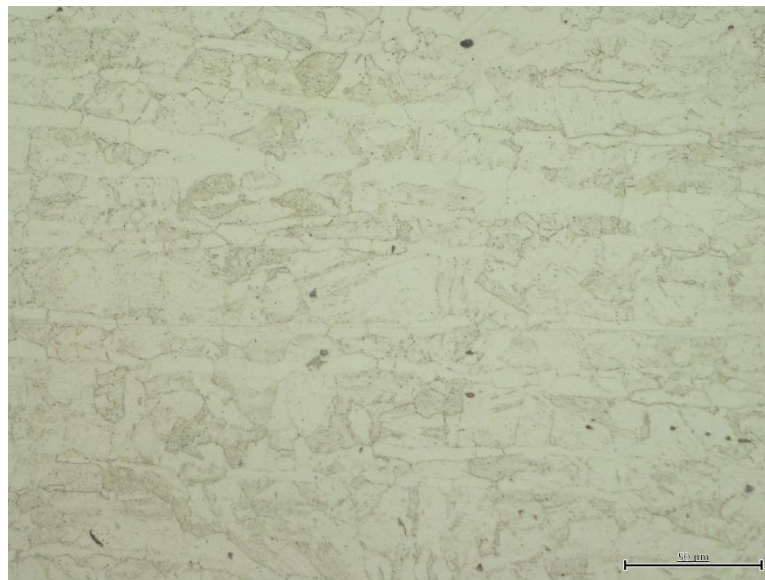
To evaluate the ultimate flexural capacity of the composite girder, the A1010 steel-concrete composite section was tested under two-point bending until failure. The measured results were compared to the hand calculations obtained from the AASHTO equations using designed and real material properties.

3.2 Material Property of A1010 Steel

The optical microscopic image of ASTM A1010 steel was obtained using Adler's 300 Series etchant, which colorized the structure, as shown in Figure 6.



a) 50×



b) 200×

Figure 6. Optical metallography of the base metal for A1010 steel

The base metal presents a dual-phase microstructure of ferrite plus austenite. As shown, the light regions represent ferrite and the dark regions represent austenite. The dark particles scattered in the images indicate the concentrations of nonmetallic inclusions.

To determine the mechanical properties of A1010 steel, such as yield strength, ultimate tensile strength, and elongation at fracture, tensile tests were conducted on three coupons under a monotonic loading scenario by using a material testing system from MTS Systems Corporation.

The geometry of the coupon samples was designed by following the standard test method according to ASTM E8 (ASTM 2016). The water-jet cutting technique was utilized for the A1010 tensile coupons that were cut from the plates located in the elastic region of the failure specimen after the ultimate bending test. Figure 7 shows the coupon sample preparation for the A1010 tensile tests.



a) Water-jet control system



b) Coupon sample cutting

Figure 7. Tensile coupon sample preparation

The MTS loading machine and its associated system were used for tensile testing. For each specimen, electricity resistance strain gauges were attached on the polished surfaces to obtain the strain and stress relationships during testing. The 0.2% offset yield strength was defined as the yield strength for the A1010 steel coupon samples. As shown in Table 4, the average yield strength and modulus of elasticity were determined to be over 68 ksi and 31,100 ksi, respectively.

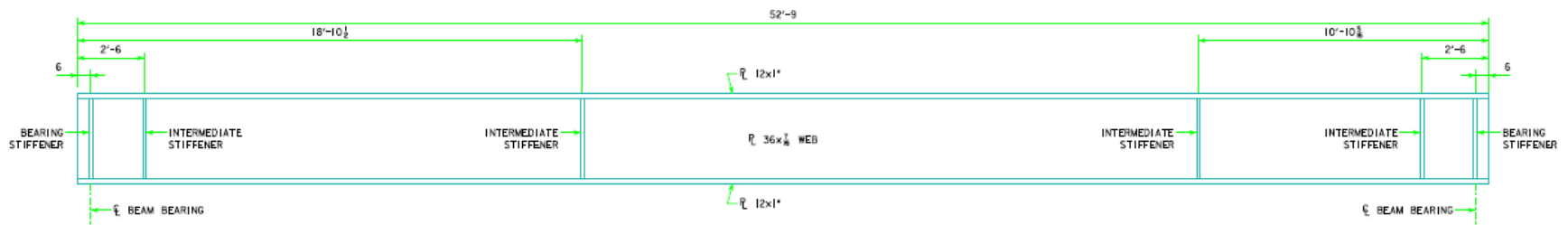
Table 4. Summary of A1010 coupon tensile test

Sample	Modulus of elasticity (ksi)	Yield strength (ksi)	Ultimate strength (ksi)	Elongation at 4 in. (%)
C-1	31,154.60	67.80	86.98	17.95
C-2	30,878.00	67.85	86.86	18.92
C-3	31,399.00	70.69	88.85	17.06
Average	31,143.87	68.78	87.56	17.98
ASTM A1010	29,000	50	70	18.0

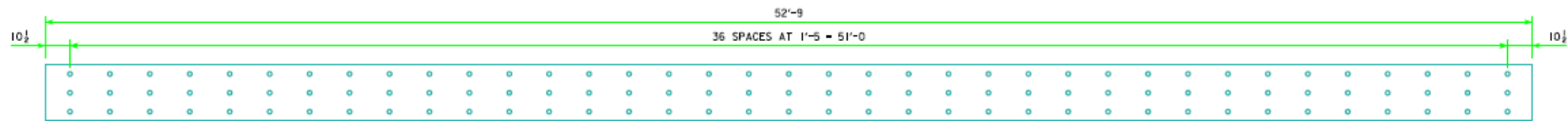
The obtained results were further compared to the minimum required mechanical properties of structural steels used for bridges as documented in the ASTM A1010/A1010M specification. As shown in the table, the tensile strength for A1010 steel, i.e., modulus of elasticity, yield strength, ultimate tensile strength, and elongation at rupture, can comply with all specification requirements.

3.2 Specimen Design Details

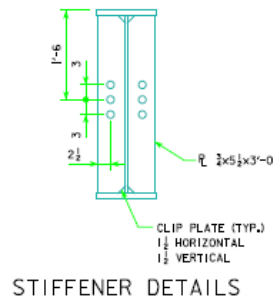
As state previously, a 52 ft 9 in. long A1010 steel girder was designed and fabricated. Figure 8 shows the plate girder profile and the section geometry for the A1010 specimen.



GIRDER ELEVATION



SHEAR STUD SPACING



STIFFENER DETAILS

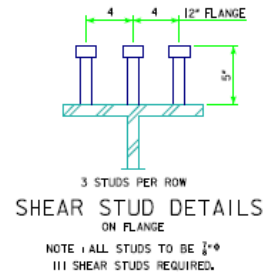


Figure 8. Details of plate girder specimen

The thickness and width of the top and bottom flange were 1 in. and 12 in., respectively. A total of 111 shear studs were welded on the top flange with 1 ft 5 in. spacing. The depth of the girder web was 36 in.

3.3 Test Setup

3.3.1 Test A – 50% Yield Moment Testing for Plate Girder

Before building a concrete deck on the top, the A1010 plate girder was first tested under two-point bending to examine the flexural performance and verify the loading system. With the goal of minimizing the chance to introduce any residual stress to the specimen, testing was limited to inducing moments in the girder subjected to only 50% of the yield moment for the plate girder.

The plate girder specimen was simply supported, loaded, and subjected to the load as shown in Figure 9.

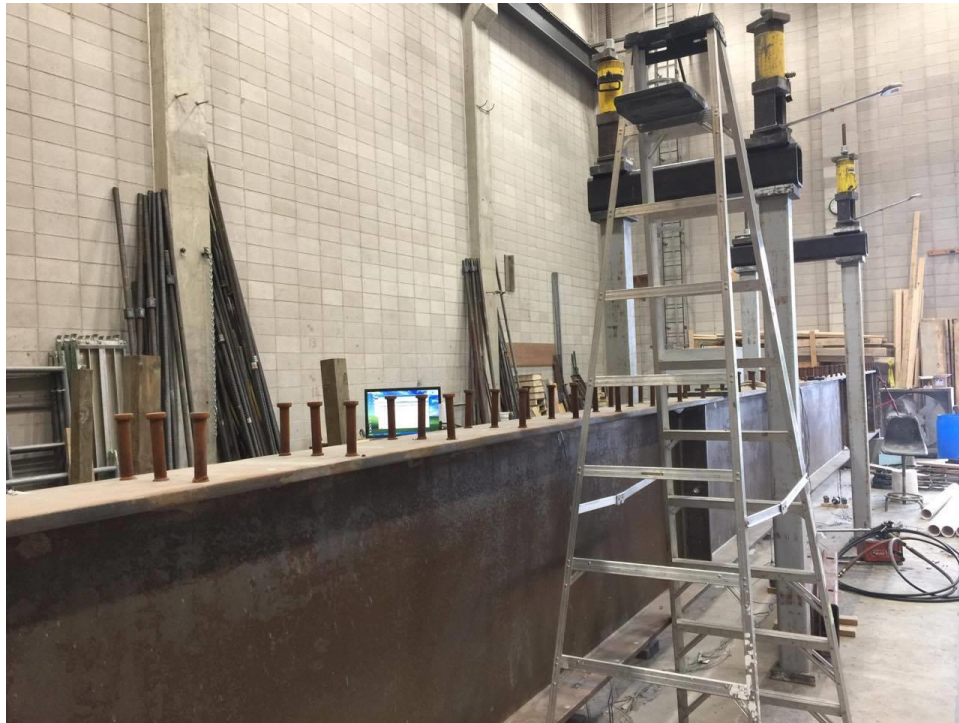


Figure 9. Loading setup for plate girder under 50% yield moment

The span was 52 ft 9 in. long, and the two loading points were spaced at 15 ft. The applied loads were recorded by two load cells installed and attached to the loading actuators. The girder was loaded up to 50 kips at each load location, which induced a moment of 1,000 kip-ft at the mid-span of the beam.

In this test, two categories of instrumentation were installed to collect data during the test: electrical resistance strain gauges (ERSGs), and displacement transducers (DCDTs). A total of 12 ERSGs, located at quarter spans and mid-span, were placed on the top and bottom flanges to obtain strain data for the plate girder. Also, a five DCDTs were placed vertically underneath the beam to record deflections under loading effects with those placed at quarter spans and mid-span, and near two end supports. The instrumentation scheme is shown in Figure 10.

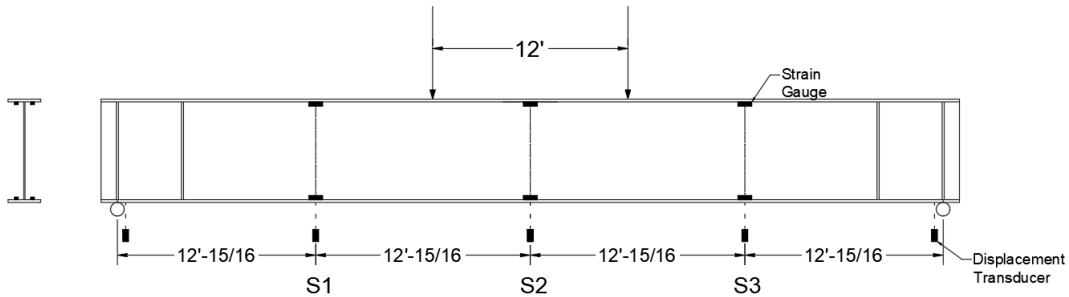


Figure 10. Instrumentation plan for Test A

3.3.2 Test B – Service Load Testing for Steel-Concrete Composite Section

After Test A, to investigate the flexural performance of the A1010 steel-concrete composite section and verify the loading system, the A1010 plate girder was subjected to a two-point bending test again with a concrete deck placed over it. The geometry of the steel-concrete deck composite beam section is shown in Figure 11.

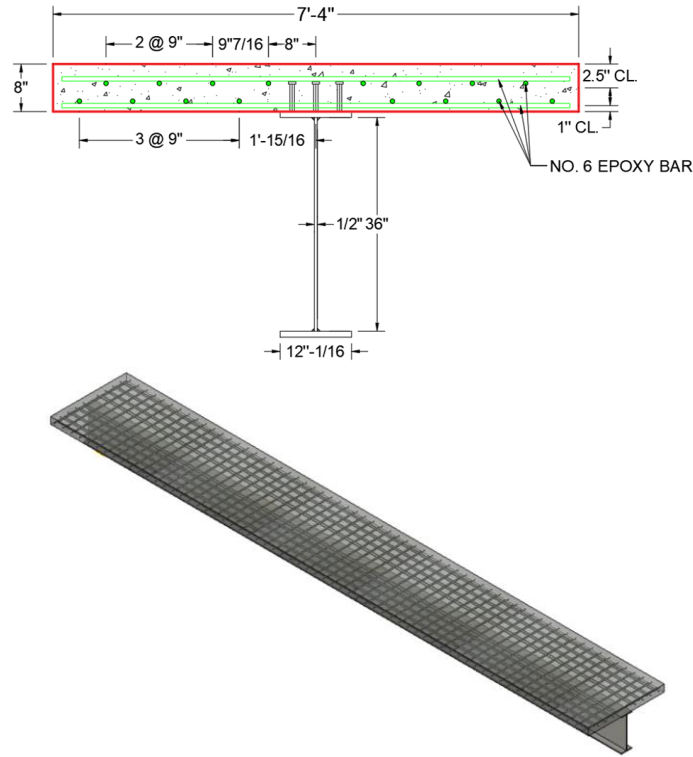


Figure 11. Geometrical dimensions and detailing of the composite beam section

The width and thickness of the deck were 7.5 ft and 8 in., respectively. Table 5 shows the compressive test results for the concrete cylinders that were obtained from the two different ready-mix trucks.

Table 5. Compression test results for concrete deck

Truck No.	Samples	Average (psi)
1	3	6,430.3
2	3	5,855.7
Combined Average	6	6,143.0

The associated modulus of elasticity was calculated using equation (2) with a 28-day compressive strength of 6,000 psi (AASHTO 2017).

$$E_c = 33,000 \times 0.145^{1.5} \times \sqrt{f'_c} \quad (2)$$

where,

f'_c is the 28-day compressive strength of concrete in ksi

Figure 12 presents the critical steps for specimen fabrication.



a) Formwork and reinforcement



b) Concrete placement



c) Deck finishing



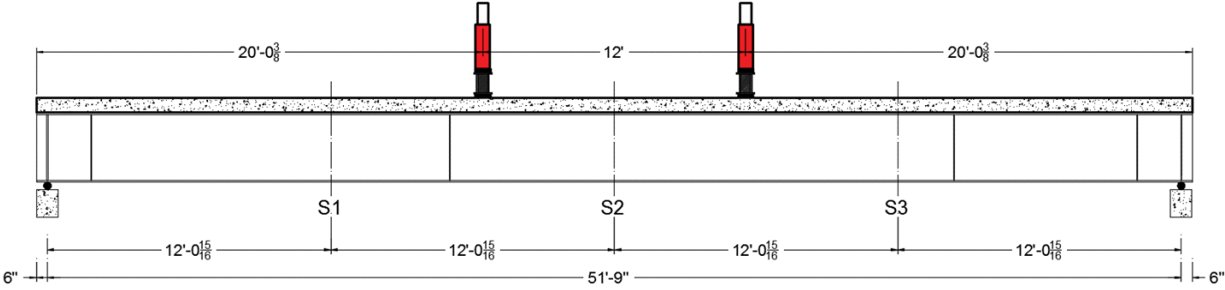
d) Deck concrete curing

Figure 12. A1010 composite beam fabrication

After curing for 28 days, the specimen was tested under a two-point bending scenario to determine the composite flexural behavior of the A1010 steel-concrete composite section.

To minimize the possibilities of introducing any residual stress, testing was limited to inducing only 50% of the yield moment for the steel-concrete composite section.

The steel-concrete composite beam was simply supported and loaded subjected to the load setup shown in Figure 13.



a) Loading scenario



b) Side view of loading setup

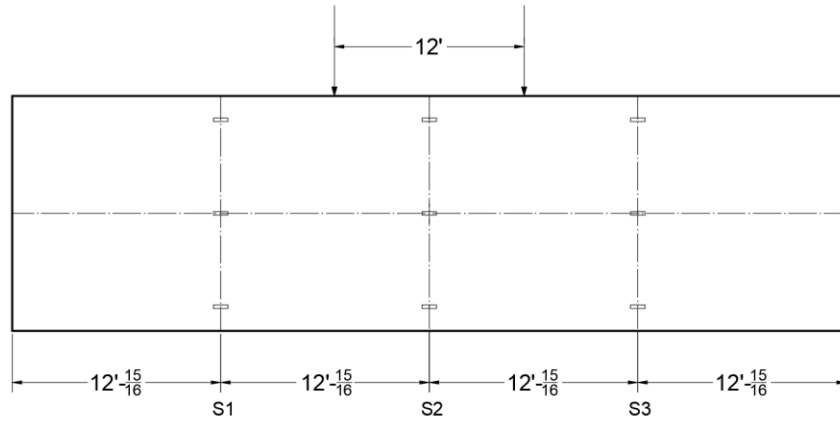


c) Bottom view of loading setup

Figure 13. Loading setup for composite beam under 50% yield moment

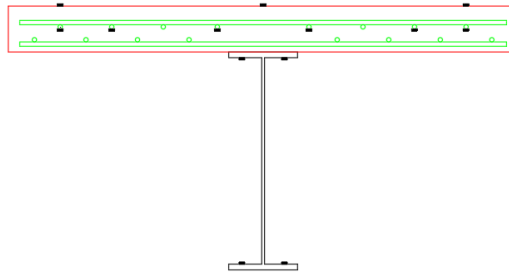
Similar to the loading setup of Test A, as shown in the figure, the span for the composite beam was 52 ft long, and the two loading points were spaced at 15 ft. The applied loads were recorded by two load cells installed and attached to the loading actuators. The girder was loaded up to 66.73 kips at each load location, which induced a moment of 1,334.6 kip-ft at the mid-span of the beam.

In this test, two categories of instrumentation were installed to collect data during the test, including ERSGs and DCDTs. A total of 12 ERSGs, located at quarter spans and mid-span, were placed on the top and bottom flange to obtain strain data for the plate girder. Another 15 ERSGs were attached on the top surface of the concrete deck and the longitudinal reinforcing steel bar in the deck to support measurement of the longitudinal strain; they were located at the mid-span. Also, five DCDTs were placed vertically underneath the beam to record deflection under loading effects; they were placed at quarter spans and mid-span and near two end supports. The instrumentation scheme is shown in Figure 14 and Figure 15.



Longitudinal Strain Gauges Placement on concrete slab for S1, S2, S3

a) Top view



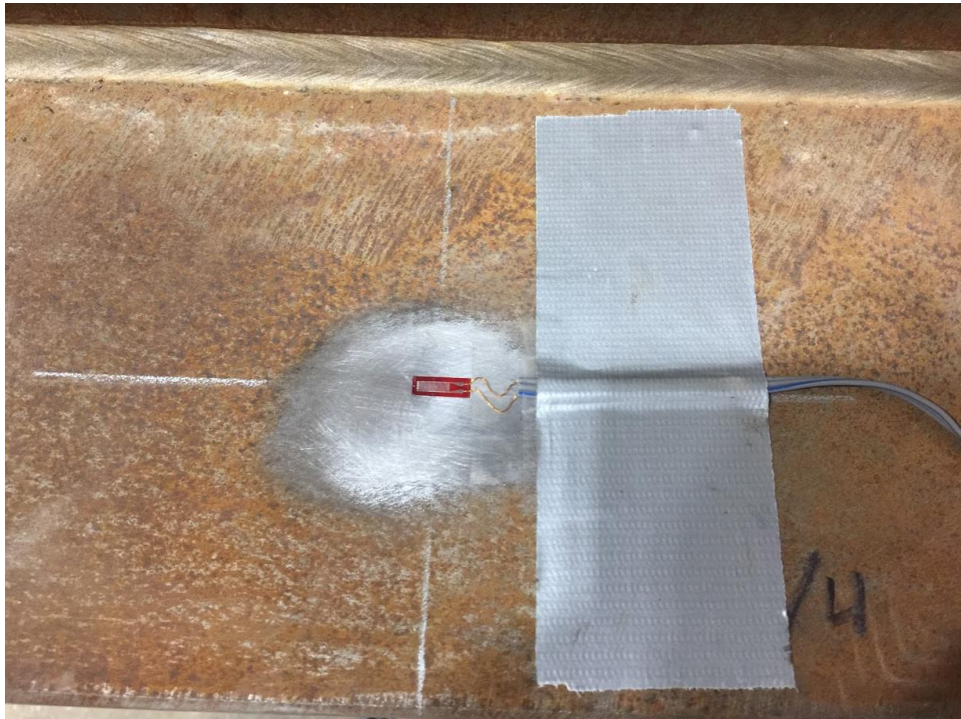
Longitudinal Strain Gauges Placement of A1010
Steel and Concrete Slab @S1, S2, S3;
Reinforcement Longitudinal Strain Gauges @S2.

b) Cross-section view

Figure 14. Instrumentation plan for Test B



a) Strain gauge arrangement on concrete deck



b) Strain gauge on A1010 steel



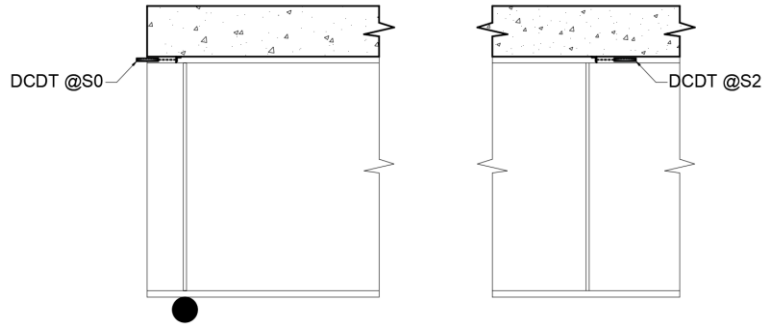
c) LVDT and DCDT at S2 (mid-span)

Figure 15. Instrumentation program

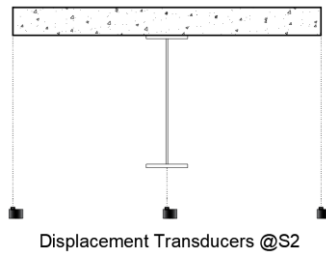
3.3.3 Test C – Ultimate Load Testing for Steel-Concrete Composite Section

After two preliminary tests were conducted and the setup was verified, Test C was performed to evaluate the ultimate flexural capacity on the same steel-concrete composite girder from Test B under two-point bending up to failure. The measured results were compared to the hand calculation obtained from the AASHTO equations using designed and real material property.

The loading setup was exactly the same as Test B. Including all the instrumentation from the previous test, two DCDTs were additionally placed at the bottom of the deck at mid-span to obtain the potential lateral-torsional buckling measurement for the specimen during the test. Two LVDTs were placed horizontally at the interface between the steel girder and concrete deck to obtain the longitudinal slip measurement during the test. They were placed at the mid-span and near to one end support. The instrumentation scheme is shown in Figure 16.



a) Two DCDTs installed at S0 (end support) and S2 (mid-span)



b) LVDTs installed at S2 (mid-span)

Figure 16. Instrumentation plan for Test C

CHAPTER 4. LABORATORY TEST RESULTS

4.1 Results of Test A

The A1010 plate girder was tested under two-point bending to verify the loading setup and the girder's flexural behavior before the construction of the concrete deck. The girder was monotonously loaded up to 50 kips at each load location, which induced a moment of 1,000 kip-ft at the mid-span of the beam. The measured test results were compared to those obtained from the hand calculations performed by following the elastic flexural theory, as shown in equations (3) and (4).

$$\delta = \frac{Pa}{24EI} (3L^2 - 4a^2) \quad (3)$$

where,

δ is the deflection at mid-span

P is the load at each location

L is the span

a is the distance between the load location and end support

E is the modulus of elasticity

I is the moment of inertia of the plate girder

$$\sigma = \frac{M \times y}{I} \quad (4)$$

where,

σ is the stress

M is the moment

y is the distance to the neutral axis

Figure 17 shows the relationship between the load-displacement curve measured from the test and that obtained from the hand calculations.

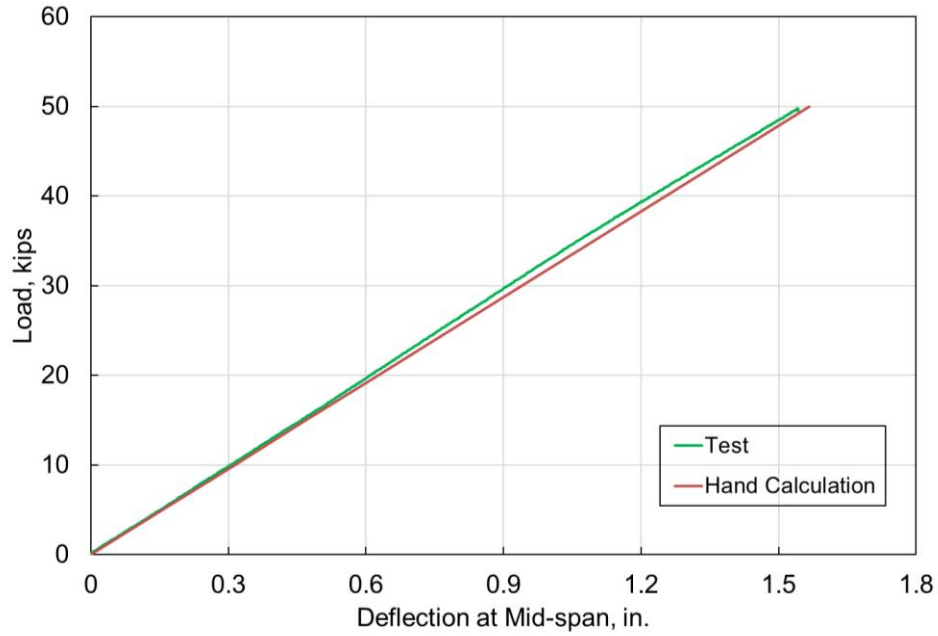


Figure 17. Load vs. displacement, Test A

As shown in the plot, displacement measured from the test was in a good agreement with that obtained from the hand calculations.

The comparison between the strain profile measured from the test and that obtained from the hand calculations subject to the load of 50 kips under Test A is shown in Figure 18.

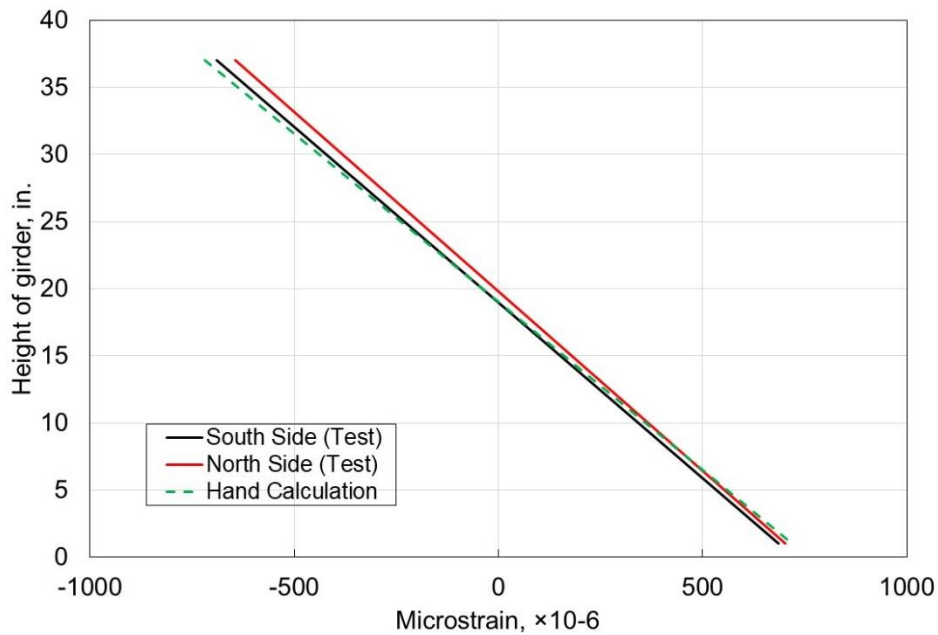


Figure 18. Strain profile under Test A (50 kips)

The associated values and difference are shown in Table 6.

Table 6. Comparison of the strain results under Test A (50 kips)

Location	Results measured from test (Micro-strain, 10^{-6})		Hand calculation (Micro-strain, 10^{-6})	Error (%)	
	North side	South side		North side	South side
	Top flange of girder	-645		-690	-719
Bottom flange of girder	702	404	719	5.0%	5.0%

As shown, other than the strain obtained from the top flange of the girder at the north side, the measured versus calculated strain values are similar. The difference may be due to an offset in load between the four actuators.

4.2 Results of Test B

As mentioned, the A1010 steel-concrete composite beam was tested under two-point bending to verify the loading setup and the girder's flexural behavior, after construction of the concrete deck. The beam was monotonously loaded up to 66.73 kips at each load location, which induced a moment of 1,334.6 kip-ft at the mid-span of the beam. The yield moment for the composite section was calculated according to equation (5).

$$f_{yt} = \frac{M_{SW}}{S_{NC}} + \frac{M_{AD}}{S_{com}} \quad (5)$$

where,

f_y is the yield stress of A1010 steel (50 ksi)

M_{AD} is the additional moment required to cause inelastic behavior at mid-span

M_{sw} is the moment induced by the beam's self-weight at mid-span

y is the distance from the centroid to the extreme tension fiber in the beam

S_{NC} is the non-composite section modulus

S_{com} is the composite section modulus

The stiffness ratio of the steel and concrete was utilized to compute the transformed section properties.

The measured test results were compared to those obtained from hand calculations, which were performed following the elastic flexural theory, as shown in equations (6) and (7).

$$\delta = \frac{Pa}{24EI_{com}}(3L^2 - 4a^2) \quad (6)$$

where,

δ is the deflection at mid-span

P is the load at each location

L is the span

a is the distance between the load location and end support

E is the modulus of elasticity

I is the moment of inertia of the composite

$$\sigma = \frac{M \times y}{I_{com}} \quad (7)$$

where,

σ is the stress

M is the moment

y is the distance to the neutral axis

Figure 19 shows the relationship between the load-displacement curve measured from the test and that obtained from the hand calculations.

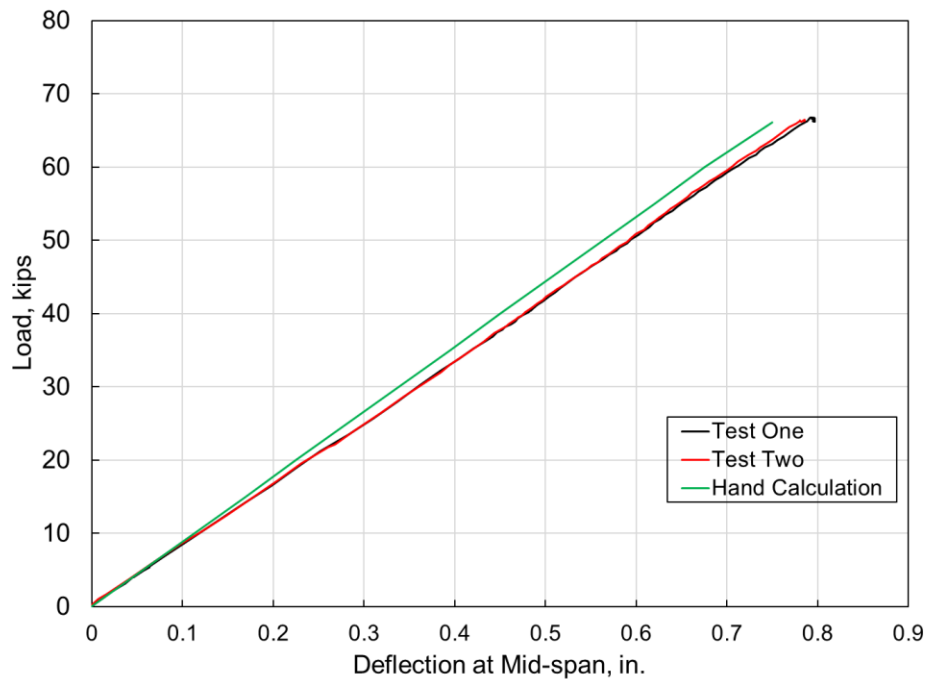


Figure 19. Load vs. displacement, Test B

There were two tests conducted for Test B. As shown in the plot, displacement measured from the test was reasonably compared with that obtained from the hand calculations.

The comparison between the strain profile measured from the test and that obtained from the hand calculations subject to the load of 50 kips under Test B is shown in Figure 20 and Figure 21.

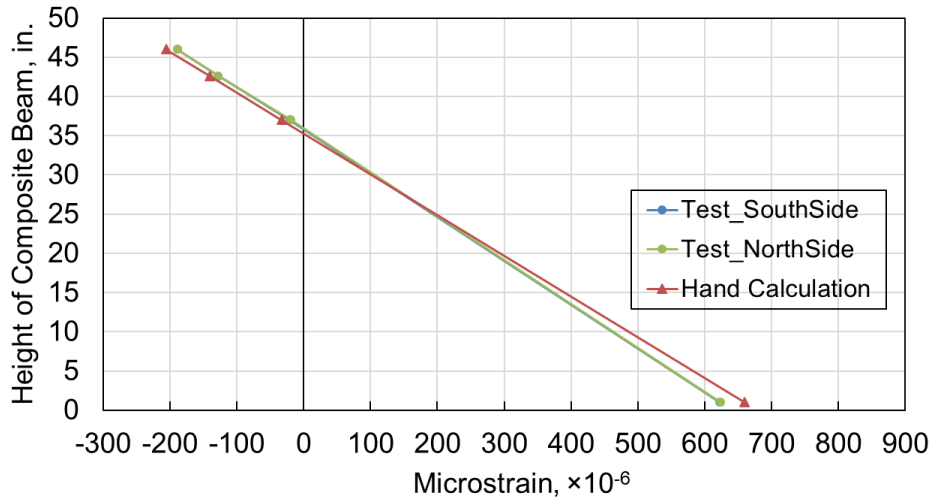


Figure 20. Strain profile under Test B (first time, 66 kips)

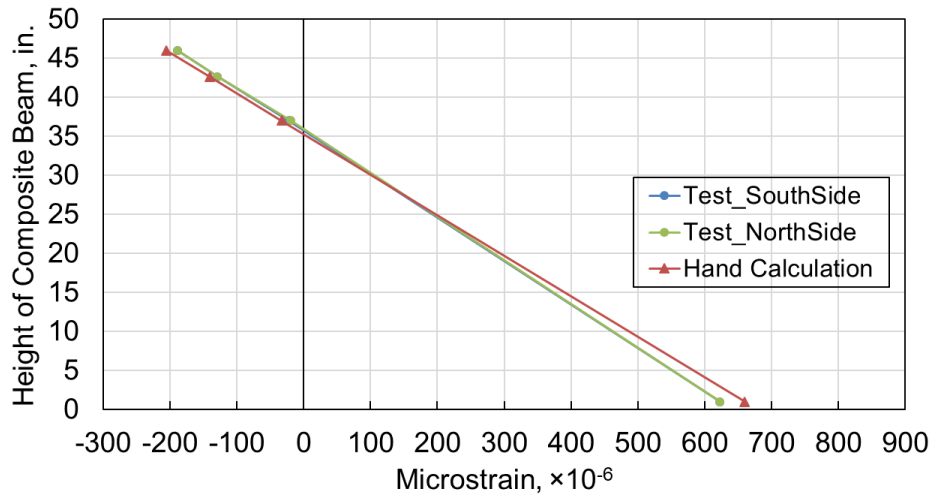


Figure 21. Strain profile under Test B (second time, 66 kips)

The associated values and differences are shown in Table 7.

Table 7. Comparison of the strain results under Test B (50 kips)

	Location	Results measured from test (Micro-strain, 10^{-6})		Hand calculation (Micro-strain, 10^{-6})	Error (%)	
		North side	South side		North side	South side
		Test One	On the deck surface	-189		-206
	On the deck reinforcements	-128		-141	10.1%	
	Top flange of girder	-19	-21	-33	-	-
	Bottom flange of girder	624	623	660	5.71%	5.87%
Test Two	On the deck surface	-189		-206	9.0%	
	On the deck reinforcements	-129		-141	9.3%	
	Top flange of girder	-19	-22	-33	-	-
	Bottom flange of girder	623	623	660	5.87%	5.87%

Note: the deck and reinforcement strain were taken as the average value measured from the strain gauges; the error was not taken into account for the strain on the top flange of the girder given the relatively small value.

The strain values measured from these two tests were similar, indicating the previous offset in load between four actuators were well prevented by attaching the continuous deck. Also, the results obtained from hand calculations were in a good agreement with those measured during testing.

4.3 Results of Test C

In addition to the laboratory tests, hand calculations were performed to compare to the test results. The hand calculations were performed using the AASHTO equations, which were based on the classic beam theory and followed by the assumption that the plane section remains plane. The stiffness ratio of the steel and concrete discussed in the previous section was utilized to compute the transformed section properties. Also, after the neutral axis of the plastic forces was located, the plastic moment capacity of the A1010 steel-concrete composite section was determined.

The general dimensions and plastic forces are shown in Figure 22.

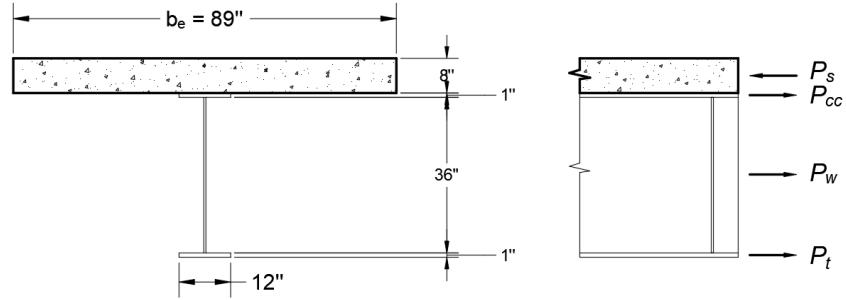


Figure 22. Plastic forces for A1010 composite section

The plastic neutral axis of the section can be computed by dividing the section into tension and compression plastic forces to obtain equilibrium.

When designed material properties were used, the plastic forces were computed utilizing equations (8) through (11).

$$P_s = 0.85f'_c b_e t_s \quad (8)$$

$$P_c = f_y b_c t_c \quad (9)$$

$$P_w = f_y D t_w \quad (10)$$

$$P_t = f_y b_t t_t \quad (11)$$

where,

P_s is the plastic force for the concrete deck

P_c is the plastic force for the top steel flange

P_w is the plastic force for the steel web

P_t is the plastic force for the bottom steel flange

f'_c is the compressive stress for concrete (4 ksi)

f_y is the yield stress for A1010 steel (50 ksi)

b_c and b_t represent the widths of the top and bottom flanges

t_c and t_t are the thicknesses of the top and bottom flanges

D and t_w are the depth and thickness of the web

When actual material properties were used, the plastic forces were computed utilizing equation (12) (Riley et al. 2007).

$$F_x = \int f_x dA \quad (12)$$

where,

F_x is the force in the x direction for each component, i.e., steel or concrete

f_x is the corresponding stress determined from the measured strain

Next, the plastic moment is the sum of the moments of the plastic forces about the plastic neutral axis. Global and local buckling were checked and assumed to be prevented so that the plastic forces can be achieved. Table 12 shows the comparison between the ultimate strength of the measurement obtained from the test and the prediction calculated from the equation from AASHTO LRFD Bridge Design Specifications.

Table 8. Comparisons between ultimate flexural strength

Comparison		Yield moment (kips·ft)	Ultimate moment (kips·ft)	Ultimate load	
				(kips)	Difference (%)
Test results		3,100.5	5,167.5	260.0	-
Hand calculations	Design property	2,651.3	4,327.5	220.0	-15.4
	Actual property	3,457.5	5,497.4	276.6	6.3

The yield moment is calculated based on the yield stress of A1010 steel sustained in the tension section below the neutral axis. The ultimate moment of the specimen under bending was calculated based on the force equilibrium theory.

As shown in the table, the predictions obtained utilizing actual material properties was reasonable compared to the results obtained from the test, which indicates the A1010 girder's ability to meet the AASHTO design requirements; when designed material properties were utilized for the hand calculations, flexural capacity measured from the test was 15.4% higher. This higher value may be due to the difference between the material properties of A1010 steel obtained from tensile tests and the recommendation in design.

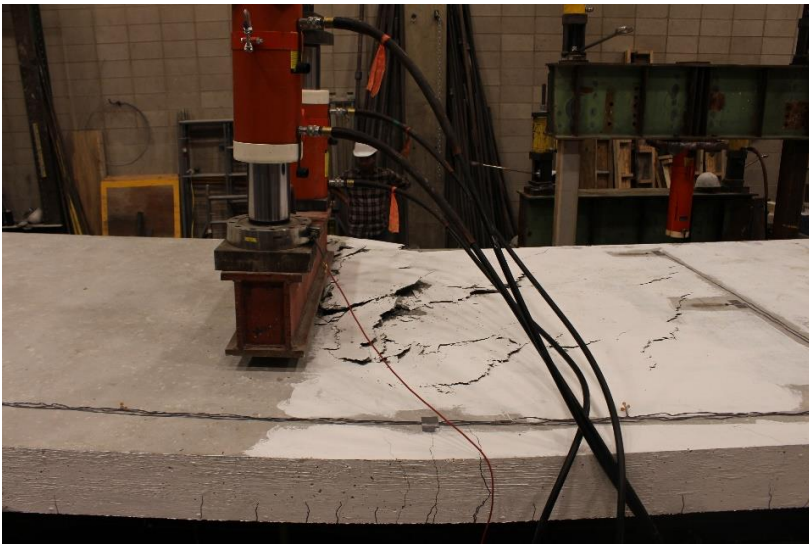
The side, bottom, and top views of the deck concrete crushing at the ultimate loading are shown in Figure 23.



a) Side view



b) Bottom view



c) Top view



d) Overall view

Figure 23. Ultimate flexural performance for A1010 specimen

A plastic deformation was observed at the ultimate loading, as shown in Figure 23, indicating satisfactory ductility for flexural behavior using the A1010 steel-concrete composite section.

The load-deflection relationship measured at S1, S2, and S3 is shown in Figure 24 and Figure 25.

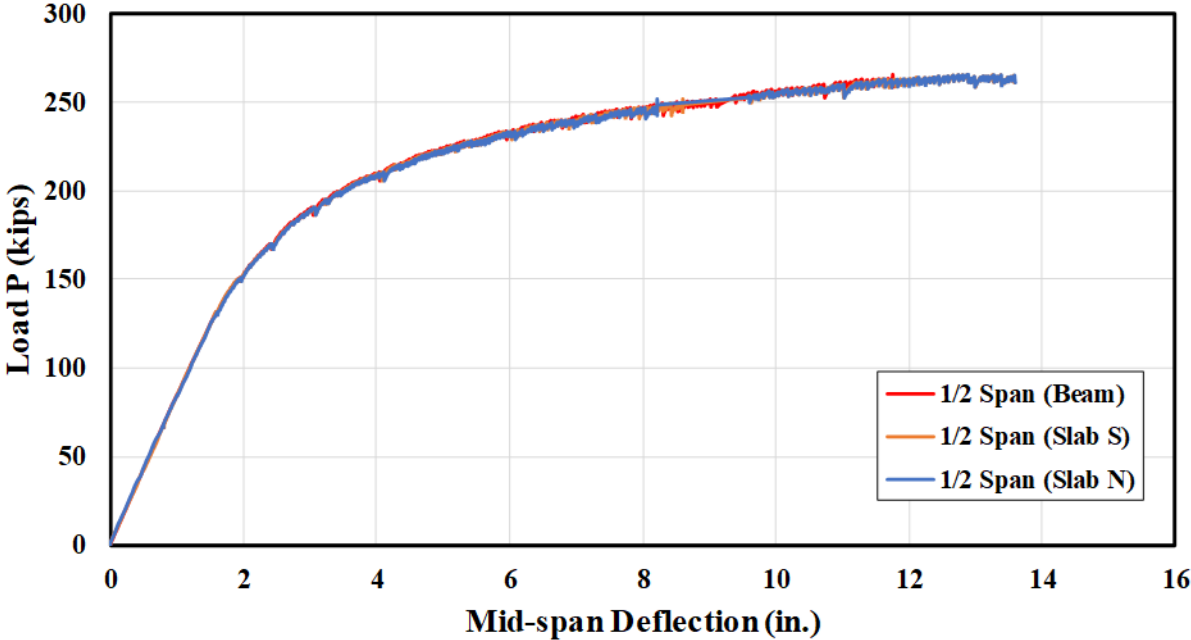


Figure 24. Maximum load-displacement curve, S2 (mid-span section)

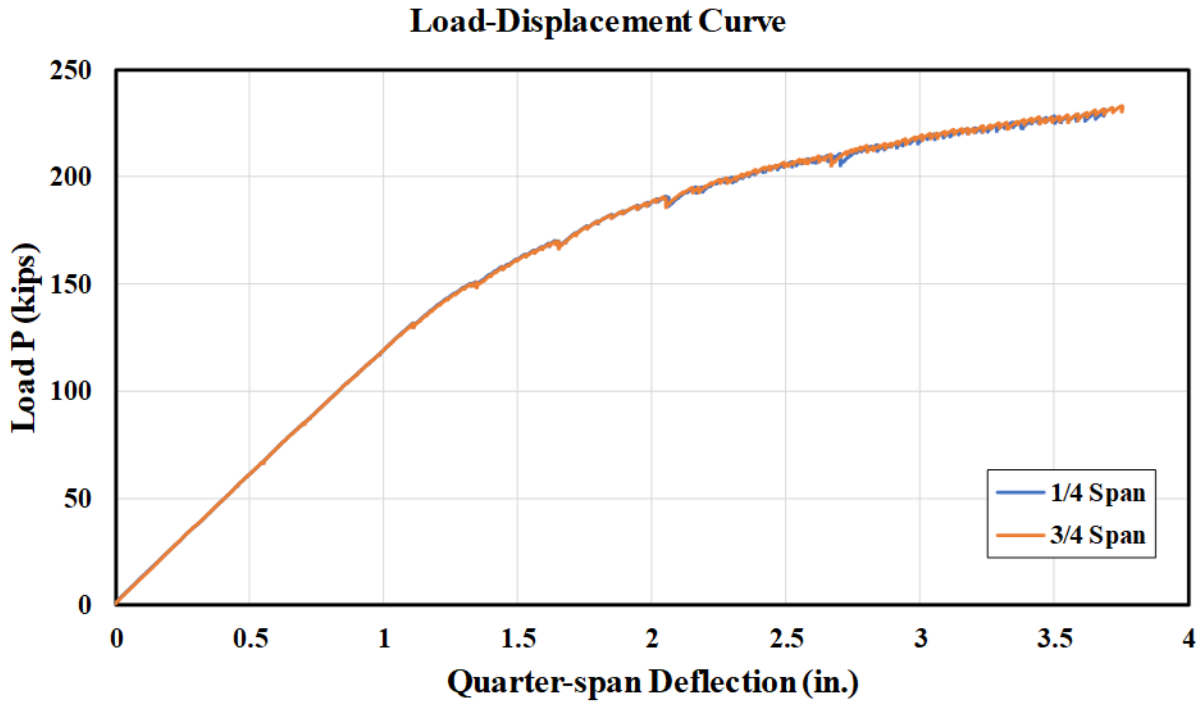


Figure 25. Maximum load-displacement curve, S1 and S3 (quarter-span sections)

As shown in these figures, no difference was observed for the load-deflection behavior measured from the bottom of the steel girder or the concrete deck. The uniformity was because the potential lateral-torsional buckling was prevented by attaching the continuous deck. Moreover, no difference was observed between the quarter spans.

At the initial stage of loading, the response of load-deflection was linear, and no cracks were found on the deck. As the load was increased, the first crack initiated at the bottom surface of the deck in mid-span, and the cracks began to propagate upward and remain normal to the beam axis. The stiffness of the beam started to degrade when the load was up to 60% P_u , indicating the specimen had reached the yield moment. When the load was increased, the cracks expanded rapidly, and the specimen reached its ultimate capacity stage. Correspondingly, spalling on the concrete deck subjected to the stress concentration was observed under the point load areas, where the beam failed because of the concrete crushing at ultimate loading.

The load and longitudinal slip relationship were measured from the LVDT and are shown in Figure 26.

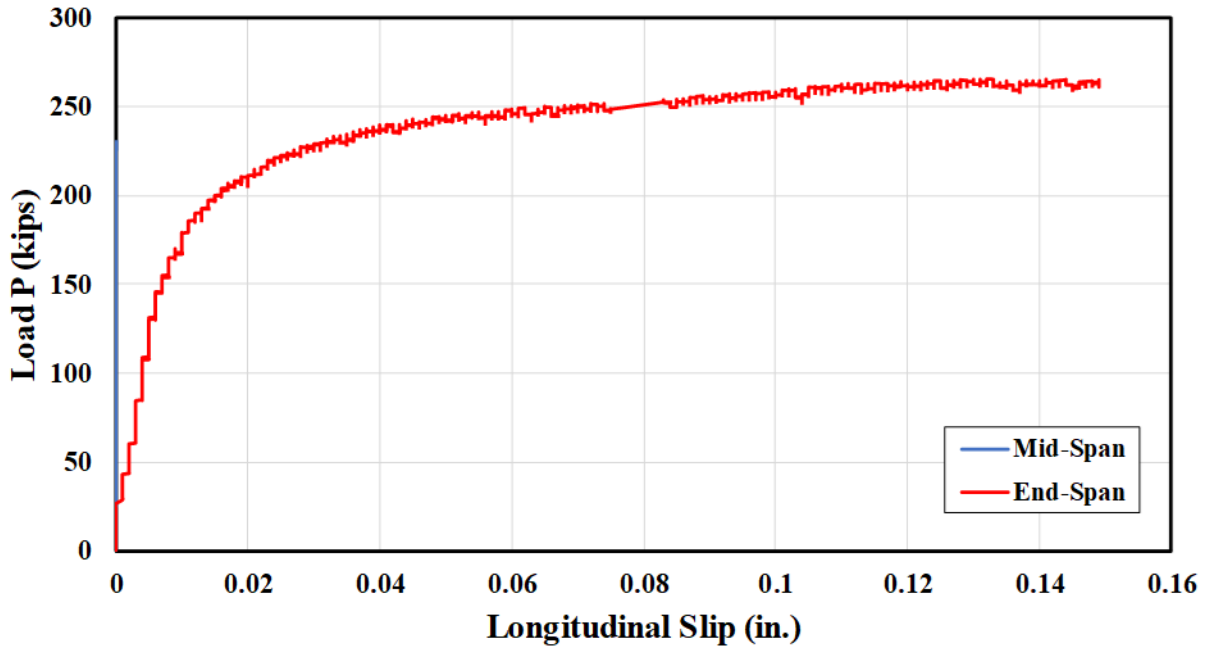


Figure 26. Load-longitudinal slip relationships, S0 and S2

As shown, the longitudinal slip at the end support increased rapidly after the specimen reached the yield point, while slip was observed to remain zero at the mid-span throughout the whole period of testing. The slip reached maximum (0.14 in.) when the beam failed.

Figure 27 presents the strain distribution subjected to bending at the mid-span cross-section.

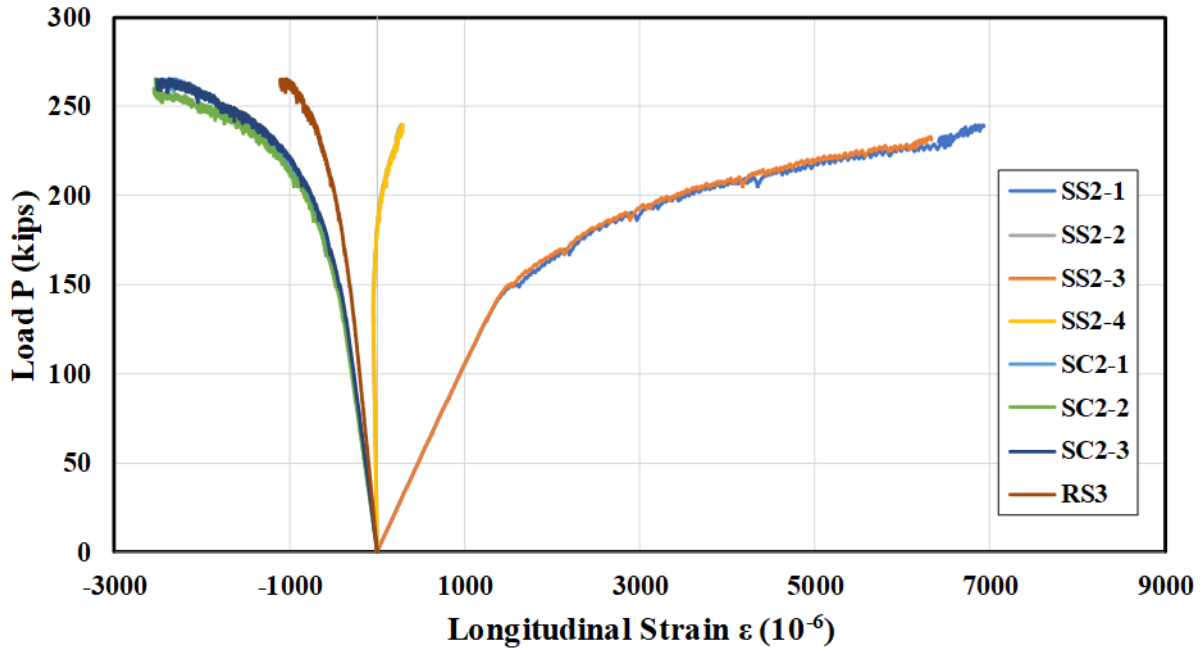


Figure 27. Longitudinal strain distribution, S2

As shown, the strain on the top flange was close to zero before the yield load; this was because it was near the neutral axis of the beam. As the load increased, the neutral axis shifted upward in the concrete deck. Correspondingly, the transverse cracks observed at the bottom surface of the concrete deck propagated due to the increased tensile stress. Also, as shown in Figure 28, in general, up to the close-to-ultimate load, the linearity of the strain distribution can be obtained, indicating that a satisfactory composite behavior had been reached.

- For Test C, the predictions obtained utilizing actual material properties were reasonable compared to the results obtained from the tests, which indicates the A1010 girder's ability to meet the AASHTO design requirements; when designed material properties were utilized for the hand calculations, flexural capacity measured from the test was 15.4% higher. This higher value may be due to the difference between the material properties of A1010 steel obtained from tensile tests and the recommendations in design.
- A satisfactory composite behavior is exhibited within the stage from the yield moment to the ultimate moment. Also, it was found that the longitudinal slip at the end support increased rapidly after the specimen reached the yield point, while slip was observed to remain zero at the mid-span throughout the whole period of testing. The slip reached maximum (0.14 in.) when the beam failed.

CHAPTER 5. FATIGUE TESTING

5.1 Introduction

Although the development of A1010 steel in the US is recent, it has rapidly gained interest for use in highway bridges (Via and Harrop 2017, Seradj 2015). Utilizing the satisfactory tensile strength of A1010 steel (i.e., 50 ksi) may not be an issue under the current design standards, because the fatigue limit state is likely to control the design.

Research to date on A1010 steel has mainly focused on design and durability aspects related to strength and corrosion resistance. Insufficient studies have focused on A1010 steel fatigue behavior. This chapter investigates the fatigue characteristics, the method of fatigue-life prediction, and their applicability to conventional fabrication using A1010 steel.

Since fatigue testing for a full-scale specimen is significantly time-consuming and costly, coupon testing and its associated mathematical model, which have been developed to predict the fatigue life, are more attractive to evaluate the fatigue resistance of A1010 steel. To predict the safe life using fatigue testing, there are two primary methods: the stress-life method (S-N curves), and the strain-life method (ϵ -N curves).

In the stress-life method, the S-N curve (i.e., the log-log plot of stress range versus the number of cycles to failure) is calculated in the elastic stress range and can be used to determine the fatigue life (Barsom and Rolfe 1999). This method is most applicable to high-cycle fatigue where the bulk material response is elastic, emphasizing nominal stresses, rather than local stresses and strains.

On the other hand, with the strain-life method, the predicted strain range is used with ϵ -N curves developed from the Coffin-Manson relation. Generally, the basic concepts in these two methods are very similar, except that the elastic-plastic strains are used to predict damage in the strain-based method (Nip et al. 2010).

In this study, the predicted S-N curve for A1010 steel was compared to the measured data from the tests. Moreover, fatigue performance was further compared to other steels including A709 weathering steel and A7 steel.

5.2 Test Program

5.2.1 Specimen Preparation

Similar to the preparation for tensile testing, the fatigue specimen was water-jet cut from the elastic region of the girder that was previously subjected to the four-point bending test. The hourglass-shaped specimens, designed according to the ASTM E466-15 standard (ASTM 2015c), are shown in Figure 29 and Figure 30.

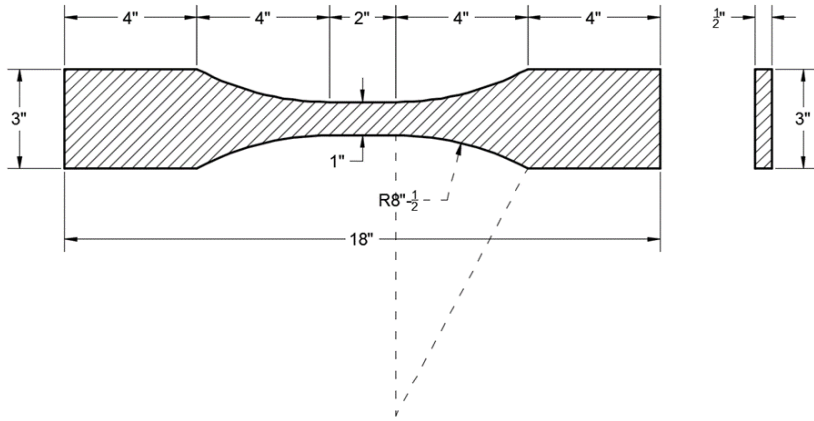


Figure 29. Hourglass shaped fatigue coupons



Figure 30. Specimens for A1010 fatigue testing

The specimens were designed to have an hourglass shape so that the local stress level changes with the cross-section. The specimens were first polished with sandpaper, and then followed by a finer polish with a high-speed wire wheel. The dimensions for the A1010 fatigue specimens are shown in Table 9.

Table 9. Dimensions of A1010 specimens and standard recommendations

Designations	T	W ₁	L ₁	W ₂	L ₂	L ₃	R	W ₁ /	L ₁ /	W ₂ /	R/	Reduced area (in. ²)
	in.							T	W ₁	W ₁	W ₁	
Specimen	0.5	1.0	2.0	3.0	4.0	18.0	8.5	2	2	3	8.5	0.5
ASTM E466	≥0.1 (as possible as)							2–6	2–3	>1.5	≥8	0.03–1.0

As shown, all of the dimensions of the fatigue coupon samples for A1010 steel were within the limitations of the standard specifications.

5.2.2 Loading Protocols

To investigate the fatigue performance of A1010 steel, each specimen was subjected to cyclic tension-compression loading under the stress-controlled protocol at room temperature. The fatigue test was performed on an MTS hydraulic machine under a sine-shaped load configuration at the stress ratio of -1 (R , min stress/max stress) and a frequency of 8 Hz (3 Hz for the load level of 75% yield stress due to the machine stability issue), as shown in Figure 31.

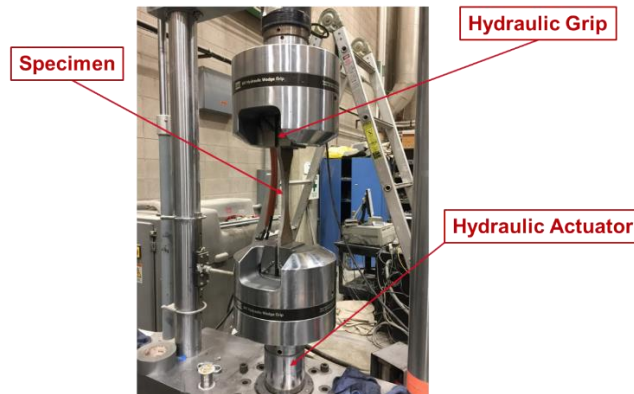


Figure 31. Fatigue testing setup

Fatigue tests were terminated when a specimen fractured or the number of fatigue cycles reached 10,000,000 cycles.

Before conducting the fatigue cyclic loading tests, a preliminary compressive test was conducted aiming to identify the buckling behavior of an A1010 fatigue specimen when subjecting it to cyclic loading protocols. The test was carried out by using the MTS machine to subject the specimen to monotonic compressive loading. A displacement transducer was attached horizontally to capture the lateral deformation. The buckling was determined when the coupon tended to deflect laterally. The buckling load was recorded as 68 ksi (equivalent to 100% yield strength of A1010 steel) when the buckling was initiated. The purpose of this test was to study the compressive and buckling behavior for A1010 fatigue coupons, with the objective to further determine the stress level for the fatigue tests.

5.3 Fatigue Testing Results

Table 10 shows the number of cycles to fracture for each of the A1010 fatigue specimens.

Table 10. Number of cycles to fracture for A1010 specimens

Coupon ID	Frequency (Hz)	Stress ratio	Max stress (ksi)	Min stress (ksi)	Thickness (in.)	Width (in.)	Area (in. ²)	Load cycles
FC2-A	8	-1	47.6	-47.6	0.520	0.990	0.515	231,991
FC3-A	8	-1	40.8	-40.8	0.520	1.001	0.521	748,801
FC4-A	8	-1	34.0	-34.0	0.519	0.999	0.518	10,000,000
FC6-A	8	-1	44.2	-44.2	0.519	1.001	0.520	288,033
FC7-A	8	-1	37.4	-37.4	0.519	0.999	0.518	10,000,000
FC8-A	3	-1	51.0	-51.0	0.523	1.000	0.523	124,689

The stress amplitude, $\Delta\sigma/2$, versus fatigue life, N_f , the fatigue behavior curve may be expressed mathematically as the following equation (13).

$$\sigma_A = a(N_f)^B \quad (13)$$

The constants a and B were obtained from a regression analysis of the tested stress- and fatigue-life data. In this study, the fatigue limit was defined as the stress amplitude level below which no fatigue failure takes place (i.e., the fatigue cycle of 10,000,000). The fatigue limit for A1010 steel subjected to high-cycle fatigue tests was identified as an S-N diagram in Figure 32.

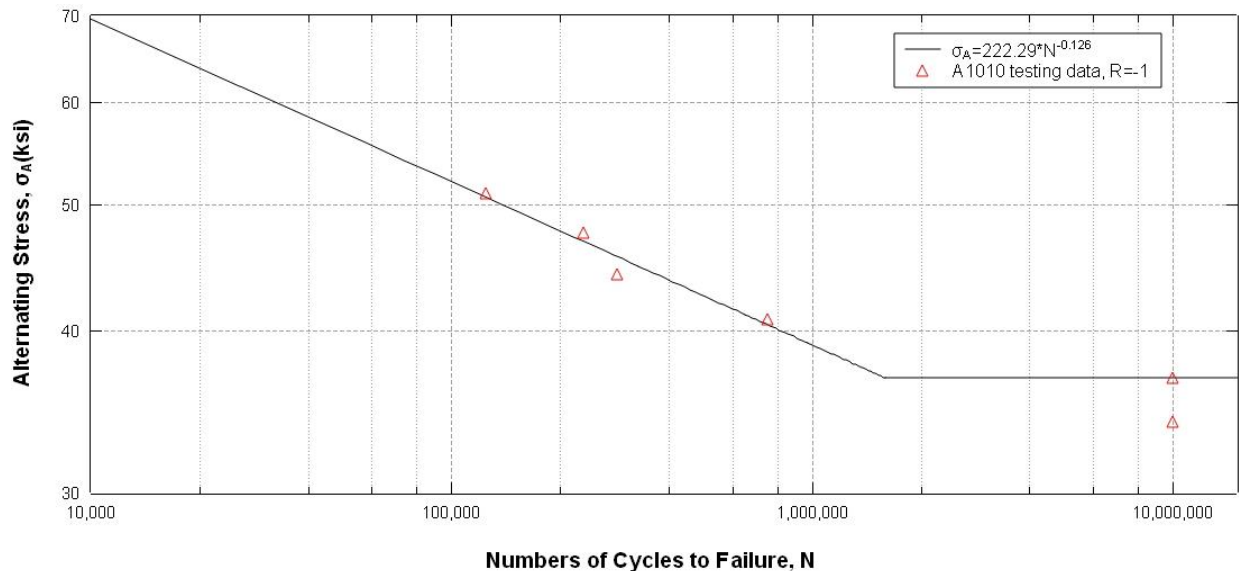


Figure 32. S-N curve for A1010 steel

The red triangles in the graph indicate the runouts, at which the fatigue-life was above 107 cycles. The fatigue limit for A1010 steel was found to be between 37.4 ksi (largest stress amplitude with no failures) and 40.8 ksi (smallest stress amplitude with failures). Therefore, it

was concluded that A1010 steel could provide adequate fatigue resistance according to current fatigue design provisions.

Furthermore, the fatigue behavior for A1010 steel obtained from the tests was compared to other conventional steels including A709 and A7 steel (Chen et al. 2007), as shown in Figure 33.

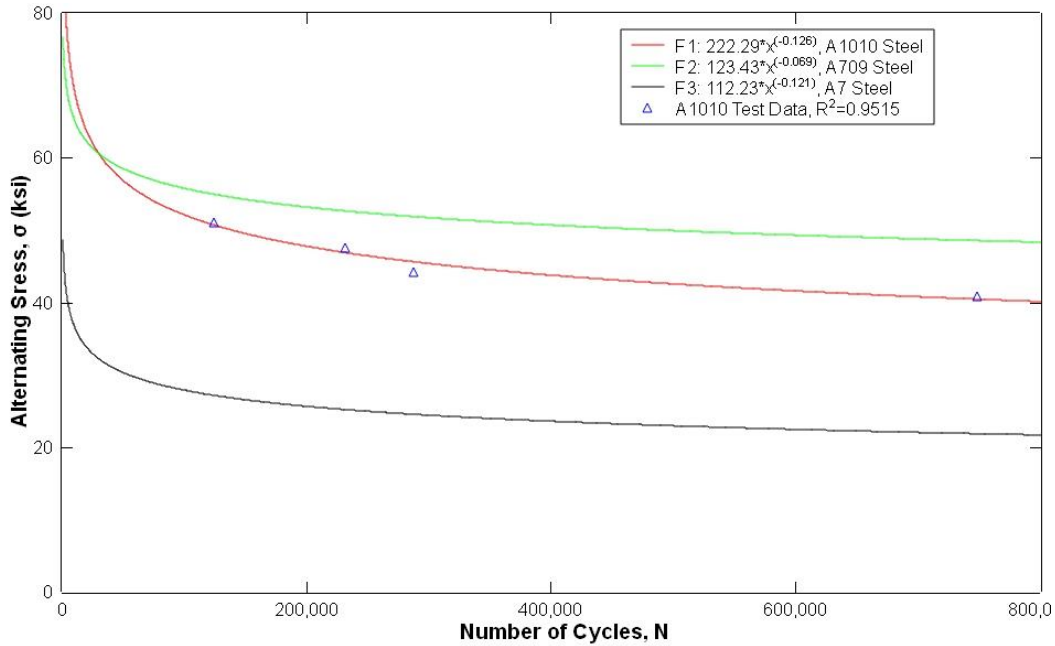


Figure 33. Comparison between S-N curve of A1010 and other steels

It was found that the A709 steel shows a slightly higher fatigue resistance in the high-cycle fatigue region than A1010 steel. Both A1010 and A709 exhibit higher fatigue resistance than A7 steel, which may be caused by the difference in their strength.

5.4 Conclusions and Recommendations

- Cyclic material tests were carried out to investigate the high-cycle fatigue properties for A1010 steel. The predicted S-N curve for A1010 steel was compared to other steel including A709 weathering steel and A7 steel.
- A709 shows a slightly higher fatigue resistance in the high-cycle fatigue region compared to A1010 steel.
- Both A1010 and A709 steel exhibit higher fatigue resistance than A7 steel, which may be caused by the difference in their strength.
- High-cycle fatigue investigations may be desired in the future for A1010 steel bolted and welded connections.

CHAPTER 6. FIELD TESTING OF THE WOODBURY COUNTY SALIX INTERCHANGE BRIDGE

6.1 Introduction

In 2016, the Iowa DOT replaced the Salix Interchange Bridge in Woodbury County with a four-span bridge constructed using both ASTM A1010 steel and A709 weathering steel. The bridge was live-load tested in the field following construction (Field Test A) and repeated one and two years later (Field Test B). The objective of these load tests was to identify any changes in behavior occurring with time. Also, data were analyzed for differences in response between the A1010 and A709 steel used.

6.2 Bridge Description

The Salix Bridge is a two-lane, four-span, continuous, steel-girder bridge located on CR K25 over I-29 (the Salix interchange). This bridge has a 17° skew and replaced the previous precast, prestressed concrete beam (PPCB) bridge. The bridge has two equal end spans with a length of 81 ft 6 in. and two equal mid-spans with the length of 120 ft. The structural steel framing plan is shown in Figure 34.

All structural steel girder material used was ASTM A709 Grade 50W, except for the two southernmost girders (E and F) that used ASTM A1010 steel. The width of the bridge roadway is 40 ft, as shown in Figure 35.

End and elevation views of the bridge are shown in Figure 36.



a) End view



b) Elevation view

Figure 36. Salix Bridge

6.3 Instrumentation Plan

The primary focus of the live load tests was to understand differences in behavior between A1010 steel girders (G5 and G6) and A709 steel girders (G1 to G4). With this intention, gauge locations were selected to capture the response and characterize the reaction through load distribution factors. Based on the characteristics of continuous bridges, strain gauges were installed on the top and bottom flange of each steel girder at three critical locations of the end span shown in Figure 38, i.e., at a distance of the girder depth to the abutment, at 0.4 of the span length, and at a distance of the girder depth to the pier.

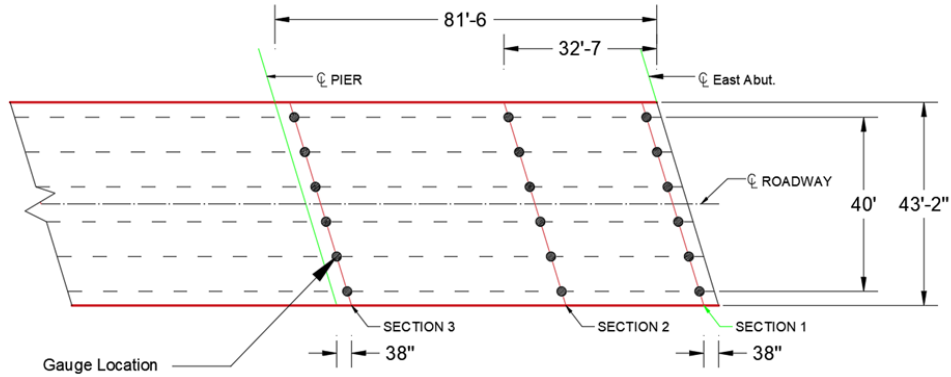
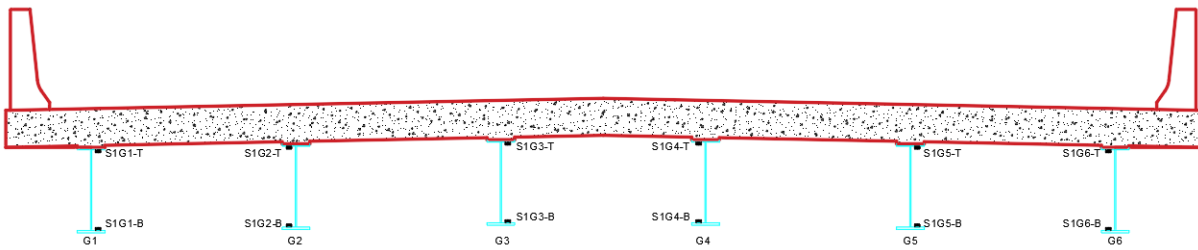
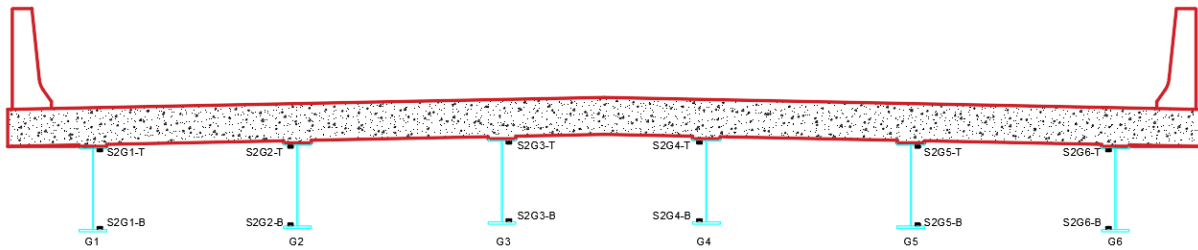


Figure 37. Plan view arrangement for instrumentation (east-end span)

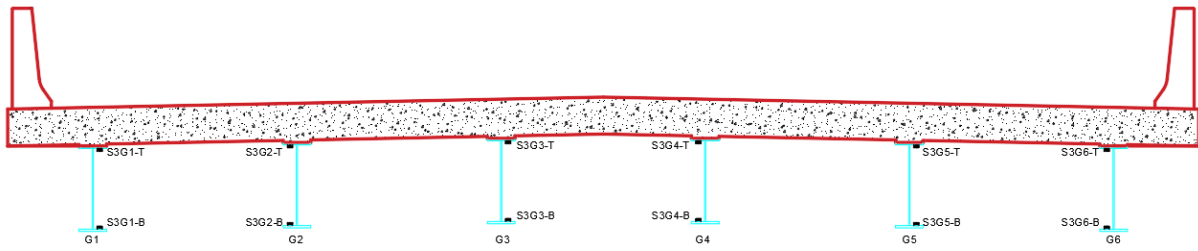
Figure 38 shows the cross-section view of the 36 strain gauge locations.



a) Section 1 (east abutment)



b) Section 2 (0.4 of span)



c) Section 3 (pier)

Figure 38. Cross-section view of strain gauge locations

Figure 39 shows close-ups of the typical instrumentation setup.



a) Strain gauge setup on A1010 steel girder



b) Strain gauge setup on A709 steel girder

Figure 39. Instrumentation setup

6.4 Loading Plan

The bridge was tested using a known tandem-axle truck. In this test, a snooper truck, provided by Iowa DOT, was utilized as shown in Figure 40.



Figure 40. Iowa DOT Salix Bridge load testing truck

The truck was also used to facilitate the instrumentation setup work. Figure 41 shows the load truck configuration and axle loads used for field testing.

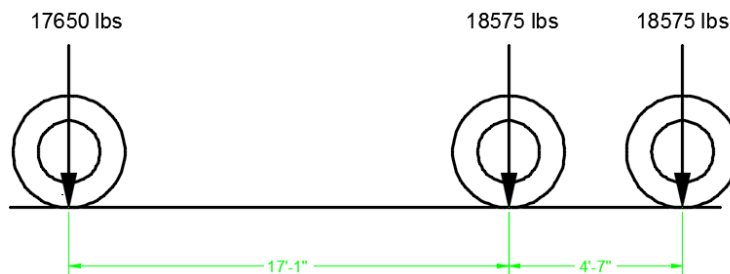


Figure 41. Configuration of loading truck and axle loads

As shown, the total weight of the snooper truck was 54,800 lb, including the front and dual rear axle weights of 17,650 lb, 18,575 lb, and 18,575 lb, respectively. The distance between the rear axles was 4 ft 7 in., and the distance from the front axle to the forward-most rear axle was 17 ft 1 in.; the front and rear axle wheelbases were 6 ft 3 in. and 7 ft 1 in., respectively.

Five longitudinal truck paths were considered for achieving the objectives of this study and were marked on the bridge deck from 1 to 5 before conducting the live load tests, as documented in Table 11.

Table 11. Loading scenarios

Load Case	Description
LC1	2 ft to the north barrier
LC2	2 ft to the center of the roadway (on A709 side)
LC3	Center of the roadway
LC4	2 ft to the center of the roadway (on A1010 side)
LC5	2 ft to the south barrier

These paths were used to guide the truck when it traveled over the bridge, as shown in Figure 42.

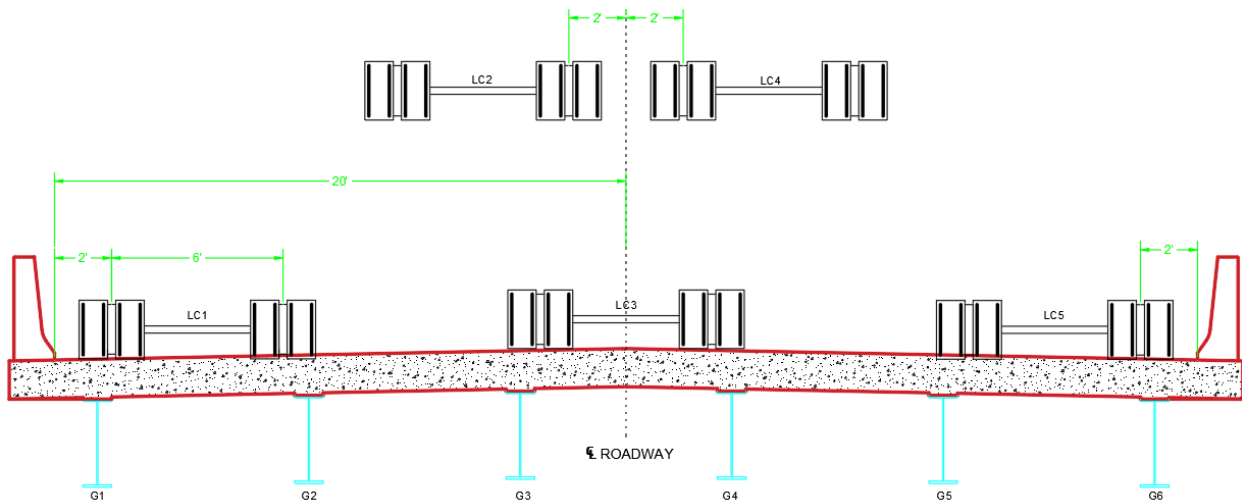


Figure 42. Truckload paths for bridge testing

Two runs were conducted for each load case, and the bridge was subjected to 10 truckload runs. For Load Case 1, the truck was driven from east to west at a crawl speed with the passenger-side wheel line offset 2 ft from the north barrier. The second load case was driving the truck from east to west at a crawl speed with the driver-side wheel line offset 2 ft from the center of the roadway of the bridge. The third load case consisted of the loaded truck driving from east to west at a crawl speed with the middle of the truck on the center of the roadway. The fourth and fifth load cases, similarly, were symmetric with Load Case 2 and Load Case 1, respectively.

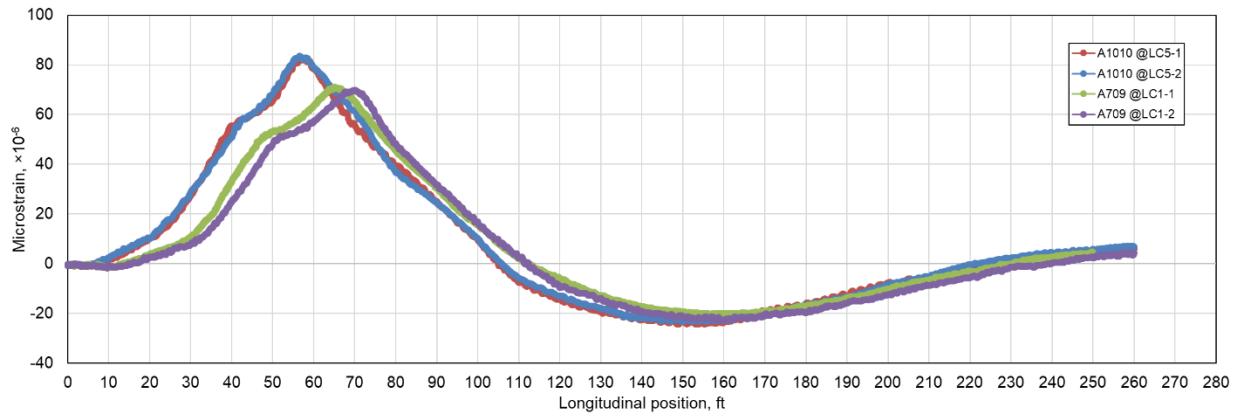
6.5 Load Test Results (2017)

This section covers the results of the 2017 load testing in the field and examines the differences in response between the A1010 and A709 steel girders.

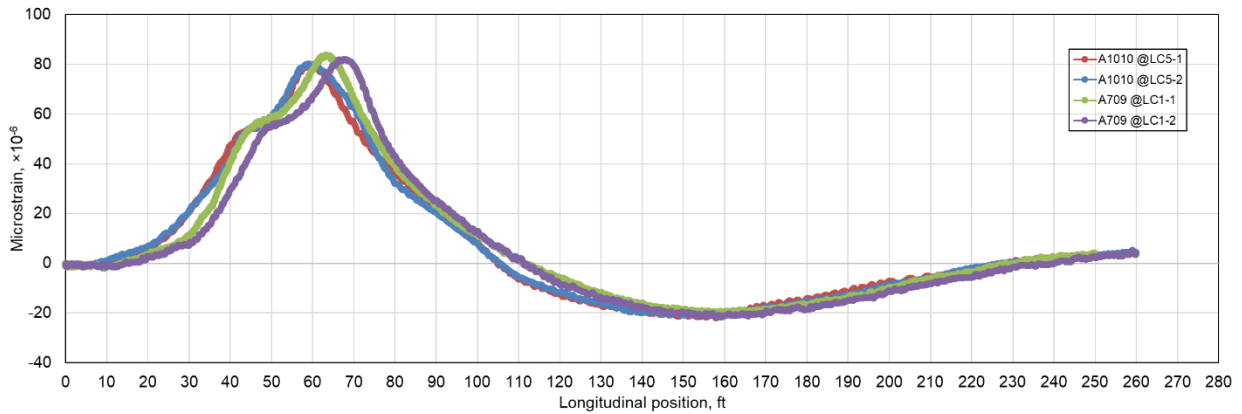
6.5.1 Comparison in Behavior between the A1010 Steel and A709 Steel

To facilitate analyses of the live load data, the girder response was determined as a function of vehicle position. Transverse lines were marked to record the longitudinal position of the truck as it crossed the bridge by painting on the deck at 10 ft intervals. The data were further plotted to show the strain response versus the longitudinal truck positions.

Figure 43 shows the strain responses versus truck position for the A1010 and A709 girders subjected to two tests for Load Case 1 and 5 in 2017.



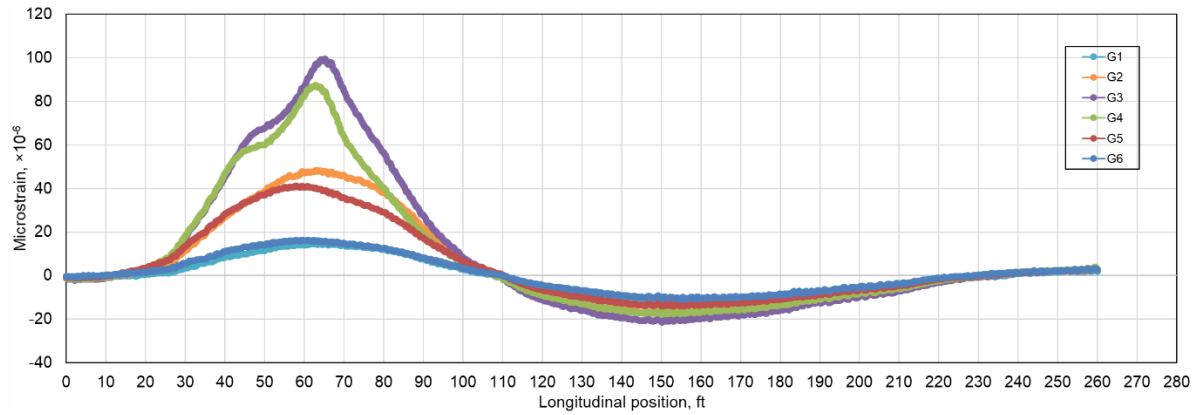
a) Exterior girder bottom flange



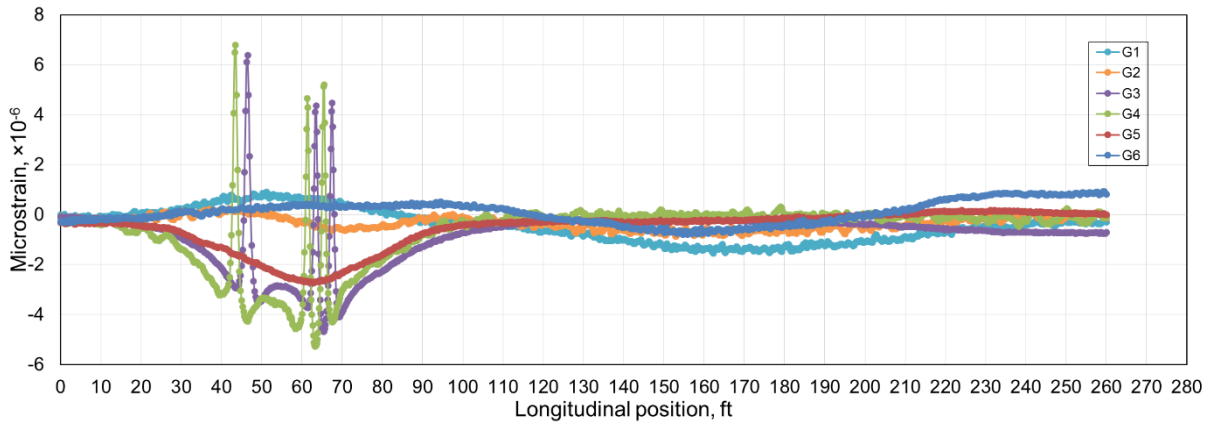
b) Interior girder bottom flange

Figure 43. Response between A1010 and A709 under Load Case 1 and 5

As shown, a slight difference (about $10 \mu\epsilon$) in the response of the exterior girder was observed between A1010 and A709 steel subjected to Load Case 1 and 5. Figure 44 shows the responses measured from the top and bottom flanges of all girders when subjected to Load Case 3.



a) Bottom flange



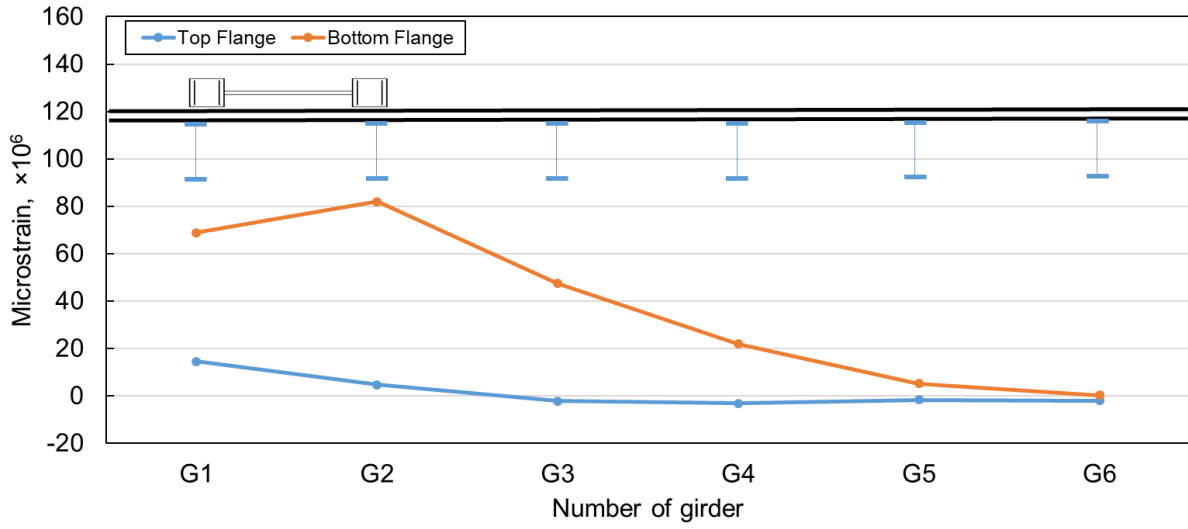
b) Top flange

Figure 44. Response of all girders under Load Case 3

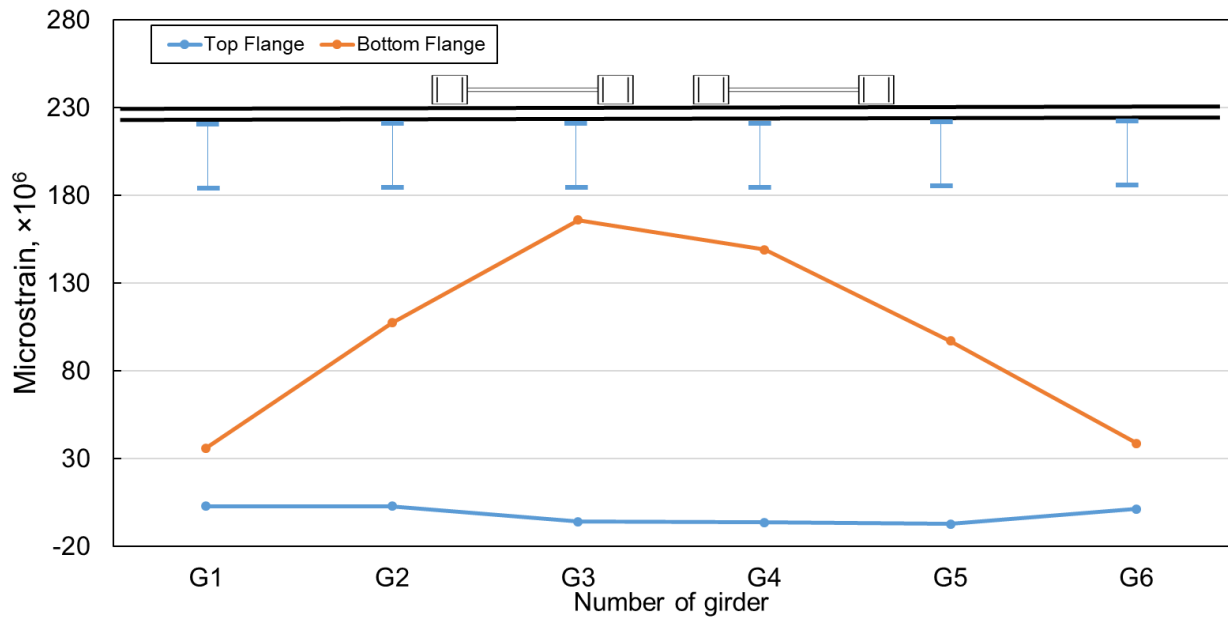
From the results, there was no difference in response to exterior/interior girders between A1010 and A709 steel subjected to Load Case 3. Comparison of the two types of girders shown in the figures indicates the A1010 and A709 girders had similar response histories concerning the corresponding load cases.

6.5.2 Distribution Factors

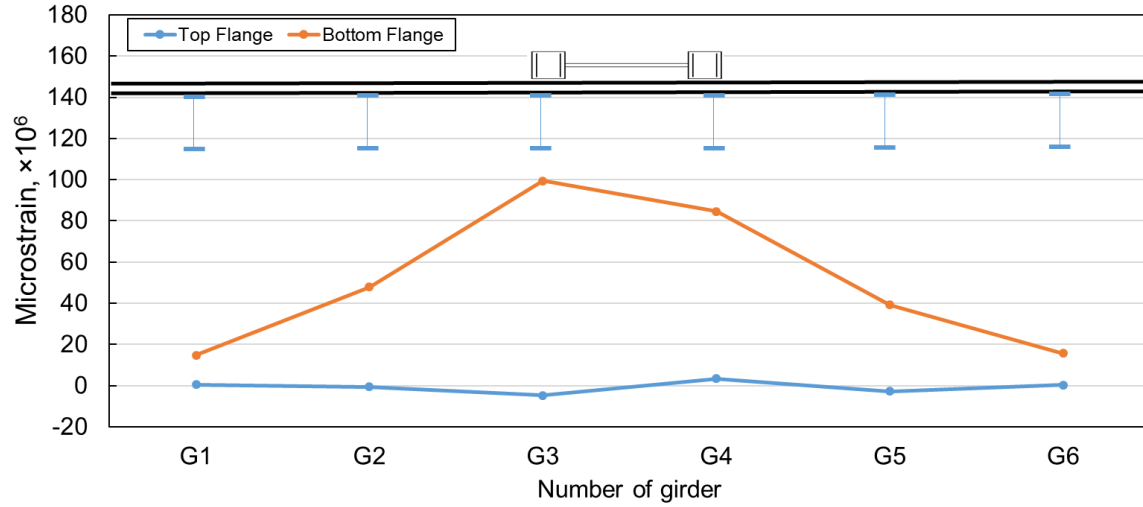
The maximum strains measured from each load case were used (with superposition of Load Case 2 and 4 for the evaluation the two-lane case) to calculate the transverse load distribution characteristics of the bridge, as shown in Figure 45.



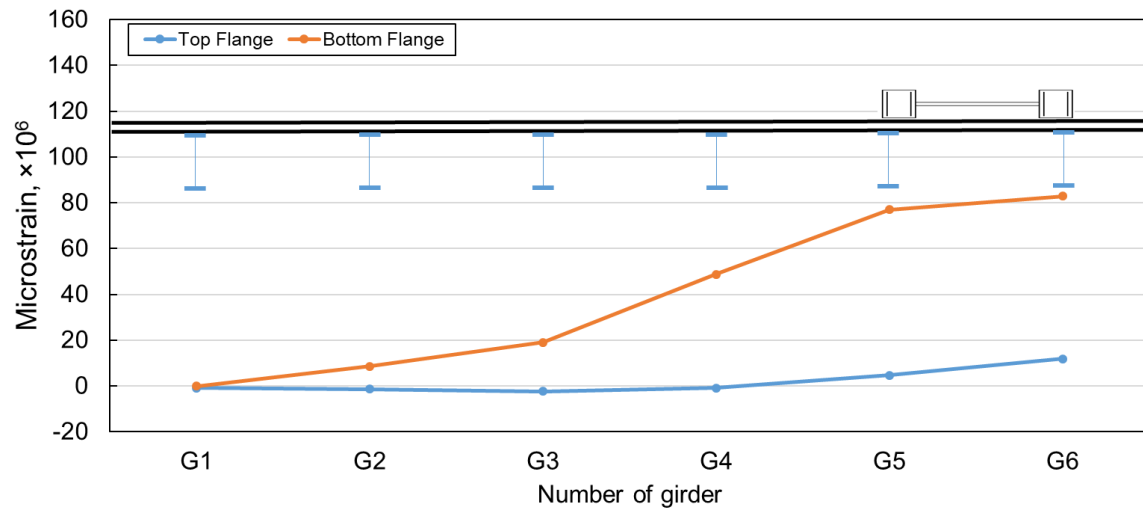
a) Load Case 1



b) Superposition of Load Case 2 and 4



c) Load Case 3



d) Load Case 5

Figure 45. Maximum strain response of all girders under each load case

Load distribution factors were computed from each load case using the maximum measured strain at the mid-span section and the following equation.

$$DF = \frac{\varepsilon_i}{\sum_{i=1}^6 \varepsilon_i} \quad (14)$$

where,

ε_i represents the maximum measured strain at bottom flange from the i th girder.

For the calculation of distribution factors, the strains on the bottom girder flange at mid-span were used. Figure 46 shows the distribution factors calculated from the measured strains and equation (14) for each load case.

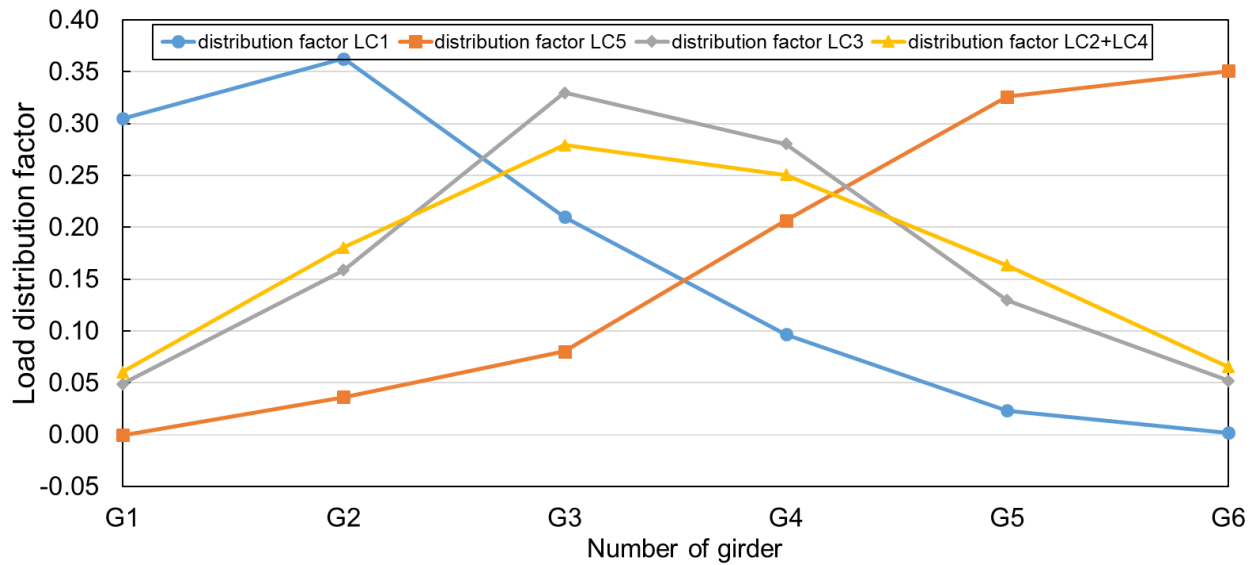


Figure 46. Measured load distribution factors under each load case

The associated calculated load distribution factors from each load case are shown in Table 12.

Table 12. Calculated load distribution factors (2017)

Load case	Girder 1	Girder 2	Girder 3	Girder 4	Girder 5	Girder 6
LC 1	0.31	0.36	0.21	0.10	0.02	0.00
LC 3	0.05	0.16	0.33	0.28	0.13	0.05
LC 5	0.00	0.04	0.08	0.21	0.33	0.35
LC 2 + LC 4	0.06	0.18	0.28	0.25	0.16	0.07

In addition to the measured distribution factors from the load tests in the field, the load distribution factors were calculated using the AASHTO LRFD Bridge Design Specifications for comparison, as shown in Figure 47.

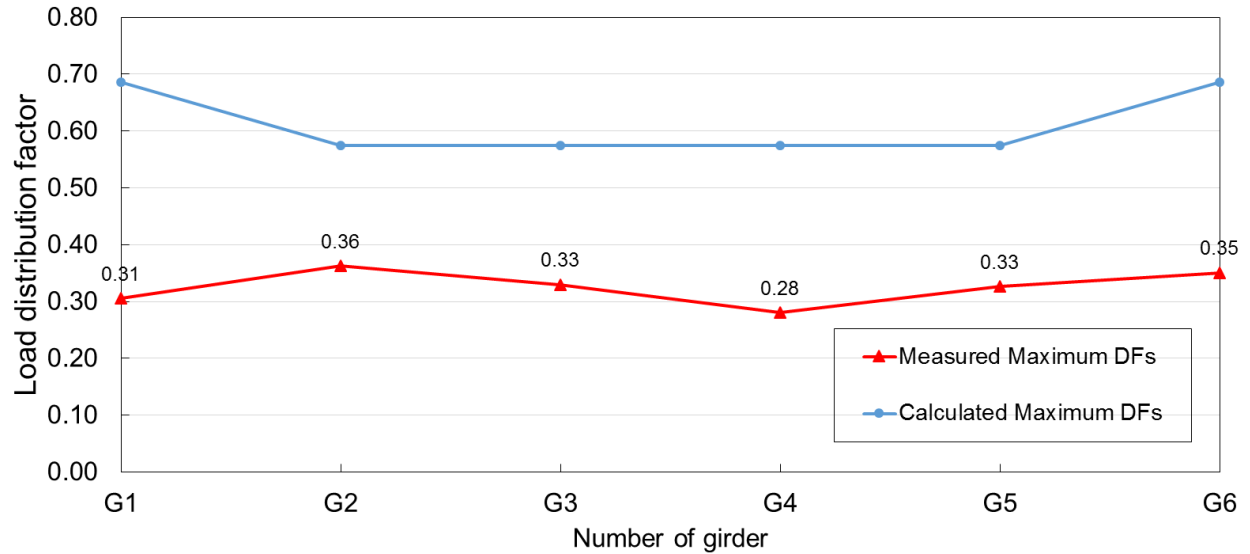


Figure 47. Comparison of experimental and AASHTO-specified load distribution factors

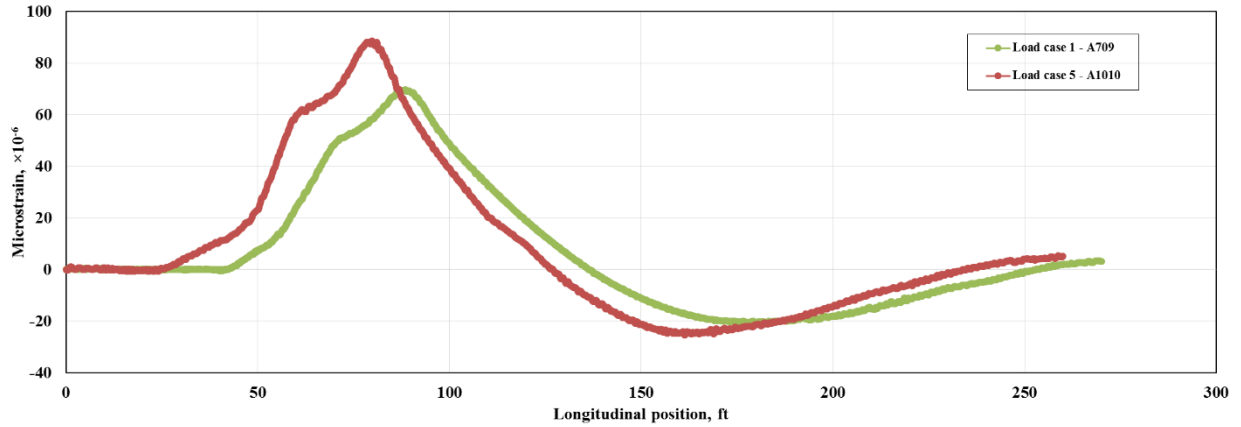
As shown in the figure, for all cases, the maximum measured distribution factors were less than those calculated using the AASHTO equations.

6.6 Load Test Results (2018)

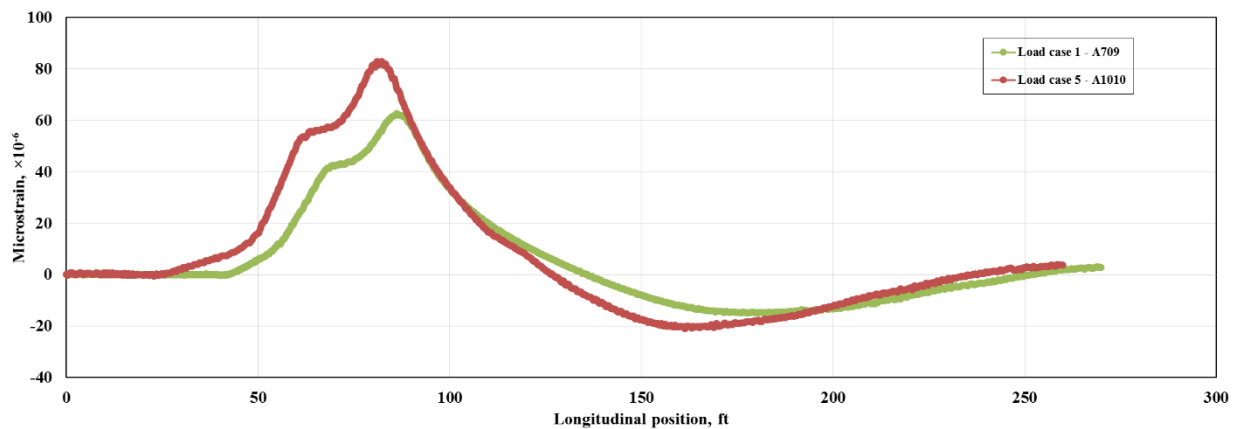
This section covers the results of the 2018 load testing in the field and examines the differences in response between the A1010 and A709 steel girders.

6.6.1 Comparison in Behavior between the A1010 Steel and A709 Steel

Figure 48 shows the strain responses versus truck position for the A1010 and A709 girders subjected to two tests for Load Case 1 and 5 in 2018.



a) Exterior girder bottom flange



b) Interior girder bottom flange

Figure 48. Response between A1010 and A709 under Load Case 1 and 5

Compared to 2017, the difference in the response of the A1010 and A709 exterior girders subjected to Load Case 1 and 5 was slightly increased (about $20 \mu\epsilon$). Figure 49 shows the responses measured from the bottom flanges of all girders when subjected to Load Case 3 in 2018.

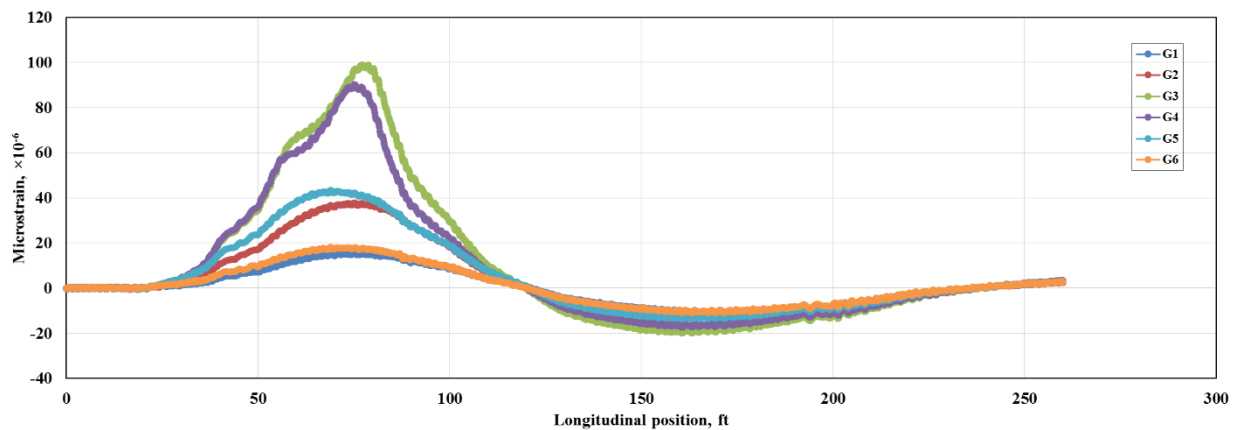


Figure 49. Response between all girders under Load Case 3

From the results, similar to the data obtained in 2017, there was no obvious difference in exterior/interior girder response between A1010 and A709 steel subjected to Load Case 3.

6.6.2 Distribution Factors

Based on equation (14), Table 13 and Figure 50 show the distribution factors calculated from the measured strains for each load case in 2018.

Table 13. Calculated load distribution factors (2018)

Load case	Girder 1	Girder 2	Girder 3	Girder 4	Girder 5	Girder 6
LC 1	0.33	0.30	0.23	0.11	0.03	0.00
LC 3	0.05	0.13	0.33	0.30	0.14	0.06
LC 5	0.00	0.03	0.08	0.21	0.33	0.36
LC 2 + LC 4	0.06	0.14	0.29	0.27	0.17	0.07

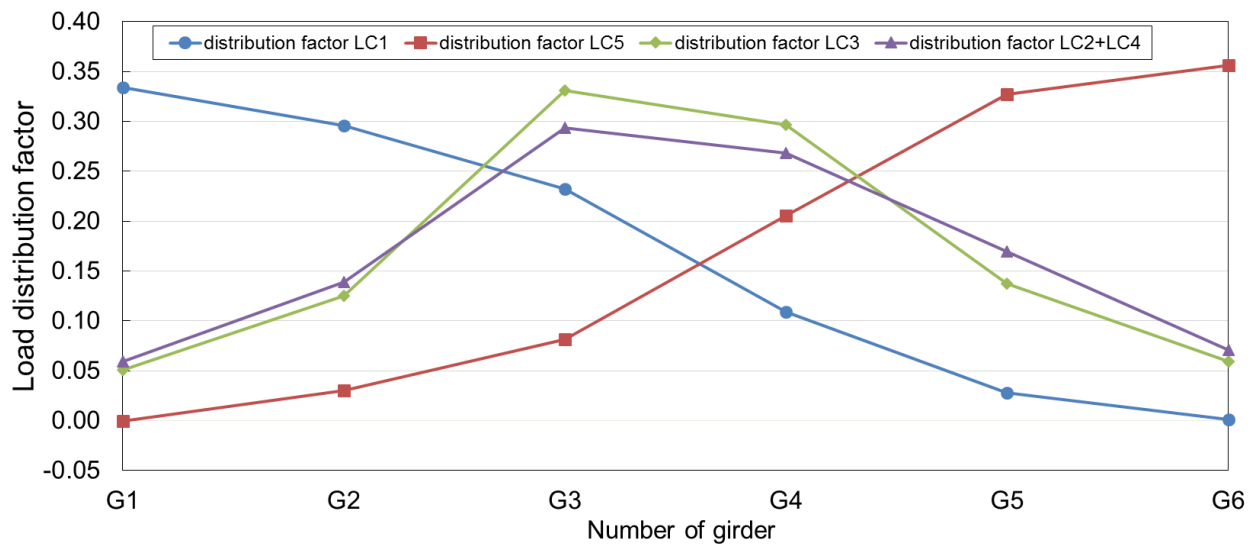


Figure 50. Measured load distribution factors under each load case

6.7 Comparison in Bridge Performance Occurring within Two Years

Figure 51 shows the measured results in 2017 and 2018 versus AASHTO-specified load distribution factors.

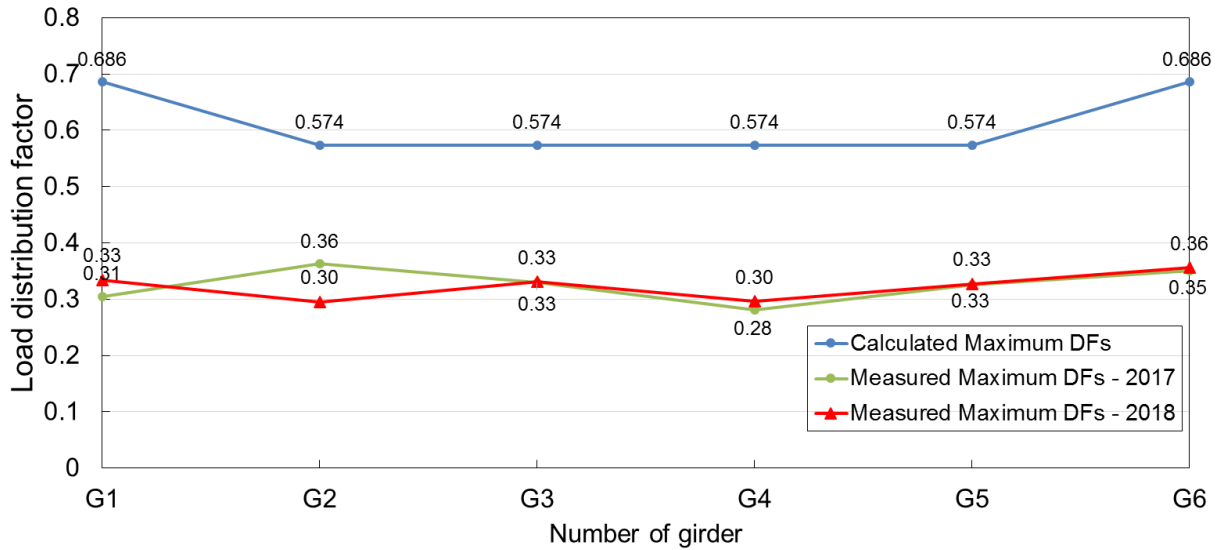


Figure 51. Comparison of distribution factors between 2017 and 2018

As shown in the figure, all of the measured distribution factors were below the code specified-value, and there was no noticeable change in the data over the two years.

6.8 Field Test Summary and Conclusions

In this project, two field tests for the Salix Interchange Bridge, which was designed utilizing A1010 and A709 steel girders, were conducted with the goal of characterizing the difference in responses between the two types of steel. Also, any changes in behavior occurring with time were identified.

From the field tests carried out in this project, the following conclusions could be drawn:

- In general, there were no apparent differences observed between the A1010 and A709 girders during the field testing.
- The calculated distribution factors from the measured field strains and the AASHTO-recommended equations were investigated for comparison. For all cases, the maximum measured distribution factors were less than those calculated using the equations.
- In general, the results showed that the changes of structural performance when subjected to static live load tests over the two years were minimal.

CHAPTER 7. GALVANIC CORROSION TESTING

7.1 Introduction

Recently, several researchers have focused on investigating the general accelerated uniform corrosion and galvanic corrosion properties of A1010 steel. However, additional tests of galvanic corrosion may be essential for A1010 steel in contact with dissimilar metals at in situ bridge sites.

To characterize the behavior of galvanic corrosion of the A1010 steel in touch with other dissimilar steel, this study implemented galvanic corrosion evaluation testing on a full-scale girder cross frame and an exposed A1010 steel plate, both of which were constructed using different types of steel bolts and welds for comparison.

This testing will be ongoing, and the longer term results will be documented and shared in the future.

7.2 Cross Frame Monitoring

Following the completion of the laboratory testing, two approximately 12 ft long sections of the girder were removed and retained to test the galvanic corrosion potential when used with two different types of bolts. Figure 52 shows the concrete deck removal from the A1010 steel-concrete composite beam.



a) Beam after concrete deck removed



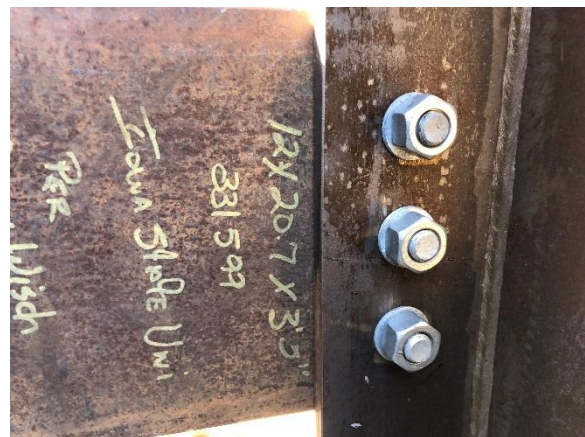
b) Concrete deck removal

Figure 52. Concrete deck removal from A1010 composite beam

The two sections of the steel beam were connected with a galvanized cross frame, as shown in Figure 53.



a) Cross frame



b) Galvanized steel bolted connection



c) Stainless steel bolted connection

Figure 53. Cross frame setup for galvanized corrosion monitoring

At one beam location, the girder and cross frame were connected using stainless steel bolts, and, on the other side, they were connected using galvanized steel bolts. The entire system was placed outside and observed for the length of the project for the development of corrosion.

7.3 A1010 Plate Exposure Testing

In addition to the galvanic corrosion of the A1010 steel cross frame, the research team worked with Justin Ocel of the FHWA regarding placement of an A1010 corrosion monitoring plate at the A1010 bridge site in Woodbury County. This plate was mounted at the bridge site during the first bridge load tests to monitor the development of corrosion. Figure 54 shows the A1010 plate being mounted in the field.



Figure 54. A1010 plate mounting in the field (December 2017)

The plate was mounted on the outside of the south barrier, in the vicinity of the east abutment. The mounting location was selected because it reduced sheltering from the bridge deck, was near the steel girder, and could be easily accessed so that future monitoring could be done without a snooper truck.

Figure 55 shows a close-up of the A1010 steel plate.

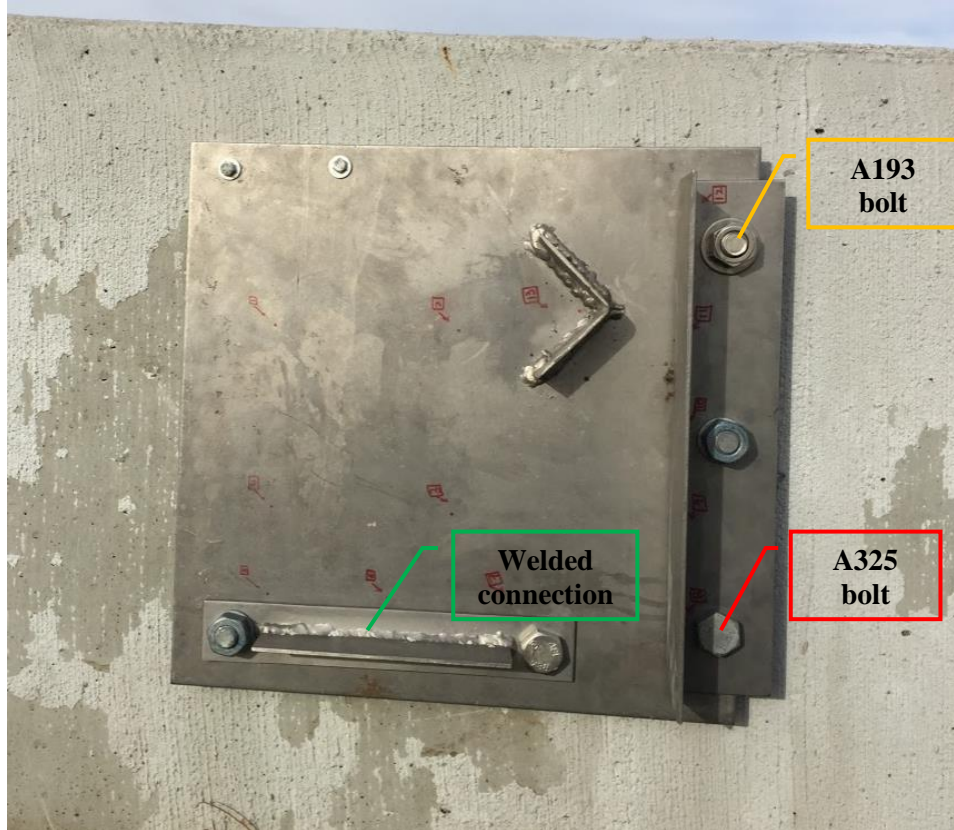


Figure 55. A1010 steel plate with stainless steel and galvanized steel bolts and welded connection

As shown, two types of bolted connections were included: an ASTM A193 stainless steel bolt and its associated nuts and washers and an ASTM A325 galvanized steel bolt and its associated nuts and washers. Additionally, a welded connection was designed to include a vertically oriented plate and an angled plate. The welding was performed with shielded metal arc welding (SMAW).

Table 14 and Table 15 show the detailed weights and measurements of each component, including the thickness of the A1010 plate.

Table 14. Weight measurements for A1010 panel

Quantity	Type	Steel	Weight (g)	Weight (lbs)
2	Bolt, washer, and nut	Stainless	505.90	1.115
3	Bolt, washer, and nut	Galvanized	733.50	1.617
1	Plate	Stainless	6,745.60	14.871
1	Angle	Stainless	1,815.20	4.002
1	T-section	Stainless	815.85	1.799
Total			10,616.05	23.404

Table 15. Thickness measurements for A1010 plate

Points	Coordinates (in.)		Thickness (in.)	Location of points
	x	y	11/28/2017	
1	12	15	0.152	
2	12	9	0.154	
3	6	9	0.154	
4	6	15	0.152	
5	3.125	15	0.151	
6	3.125	11	0.154	
7	3.125	7	0.154	
8	3	2	—	
9	6	2	0.152	
10	9	2	—	
11	12	2	0.152	
12	16	2	0.153	
13	12.875	5	0.155	
14	12	see detail	0.151	
15	6	see detail	0.148	
16	see detail	8	0.158	
17	see detail	13	0.157	

Thickness/weight loss data will be monitored as the average thickness/weight loss per year during the ongoing testing period. A comparison between the corrosion behavior of the stainless and galvanized steel bolts will also be investigated.

7.4 Ongoing Corrosion Measurements

The two test specimens were atmospherically exposed to provide essential information on the serviceable lifetime for an A1010 steel bridge until maintenance is required. Furthermore, the results will provide data to understand the importance of controlling and reducing the galvanic corrosion for future A1010 steel bridges located in the region. To achieve this goal, the following measurements and evaluation will be carried out with the results documented in a future report.

- **Cross-frame specimen**

During the proposed 30-year exposure period, pitting and rust formation will be observed, recorded, and compared between the two bolted connections, i.e., the stainless and galvanized steel bolts..

- **A1010 research plate**

During the proposed 30-year plate exposure period, thickness measurements will be recorded at each visit to the site. Additionally, rust formation for the different connections, i.e., stainless steel bolt, galvanized steel bolt, and welding on the plate, will be recorded.

The data and analysis will be presented in a future report, which will assess the pitting and rust formation as well as the galvanic behavior for the bolted cross frame and the A1010 steel plate during the entire exposure time.

CHAPTER 8. SUMMARY, CONCLUSIONS, AND RECOMMENDATIONS

8.1 Summary

In 2016, the Iowa DOT replaced a bridge in Woodbury County (on CR K25 over I-29) with a four-span bridge partially constructed using ASTM A1010 bridge steel. The goals of this project were to evaluate the fundamental behavior of girders fabricated using A1010 steel, evaluate the potential for galvanic corrosion when various fastener types are used, and assess the in situ performance of the Woodbury County Salix Interchange Bridge.

A comprehensive laboratory program was carried out to investigate the performance of A1010 steel under a four-point bending scenario to determine the plate girder and composite flexural behavior. For this purpose, a 52 ft 9 in. long girder was designed, fabricated, and laboratory tested while subjected to four-point bending, with the results compared to the current AASHTO LRFD Bridge Design Specifications. Additionally, tensile and fatigue tests were conducted to obtain the mechanical and fatigue behavior for the A1010 steel.

Live load tests for the bridge were also conducted in the field to identify any changes in behavior occurring with time. Data were analyzed for differences in response between the A1010 and A709 steel girders.

8.2 Conclusions

From the work carried out in this study, the researchers came to the following conclusions:

- The predictions obtained utilizing actual material properties were reasonable compared to the results obtained from the laboratory test, indicating the A1010 girder's ability to meet the AASHTO design requirements. When the designed material properties were utilized for hand calculations, the flexural capacity measured from the laboratory test was 15.4% higher. This may be due to the difference between the material properties of A1010 steel obtained from tensile tests and the recommendations in design.
- The fatigue limit for A1010 steel was found to be between 37.4 ksi and 40.8 ksi. Thus, A1010 steel can provide adequate fatigue resistance according to current fatigue design provisions.
- In general, there were no apparent differences observed between A1010 and A709 girders during field testing. Additionally, the calculated distribution factors from the measured field strains and the AASHTO-recommended equations were investigated for comparison. For all cases, the maximum measured distribution factors were less than those calculated using the equations.

- Load tests performed on the A1010 steel bridge over two years indicated that the bridge constructed using A1010 and A709 steel girders performed well.

8.3 Future Work

Although it was concluded that the A1010 steel shows satisfactory structural and fatigue performance, further field studies are being conducted to evaluate the potential for galvanic corrosion when different types of bolts and welds are used.

To achieve this goal, a future study will be carried out on the following:

- Long-term observational monitoring of galvanic corrosion on the full-scale cross frame will collect data for two types of bolted connections: stainless steel bolts and galvanized steel bolts.
- Long-term monitoring of the A1010 steel plate placed at the bridge site will be conducted and periodically documented for the development of corrosion. The data and analysis will be presented in a future report, which will assess the galvanic behavior for the A1010 plate throughout the exposure time.

The results of this work will help in understanding the importance of controlling and reducing galvanic corrosion for future A1010 steel bridges located in the region.

8.4 Recommendations for Additional Future Research

The following recommendations are provided for future study based on the observations from this project:

- Long-term monitoring of galvanic corrosion behavior may be necessary to be performed for A1010 welded connections
- High-cycle fatigue investigations may be desired for A1010 steel bolted and welded connections

REFERENCES

- AASHTO. 2017. *Load and Resistance Factor Design (LRFD) Bridge Design Specifications*. Eighth Edition. American Association of State Highway and Transportation Officials, Washington, DC.
- Albrecht, P. and A. H. Naeemi. 1984. *NCHRP Report 272: Performance of Weathering Steel in Bridges*. National Cooperative Highway Research Program, Washington, DC.
- ArcelorMittal. 2010. *Stainless Steel and Corrosion*. ArcelorMittal Stainless Europe, Paris, France.
- ArcelorMittal. 2010. *Duracorr®: Welding Guidelines*. ArcelorMittal USA, Chicago, IL. <https://iowadot.gov/bridge/A1010/Presentations/ARCELORMITTAL%20DURACORR%20WELDING.pdf>.
- ArcelorMittal. 2013. *Duracorr®/A1010: Bridge Applications and Fabrication Guidelines*. ArcelorMittal USA, Chicago, IL. <https://iowadot.gov/bridge/A1010/presentations/arcelormittal%20duracorr%20bridges.pdf>.
- ArcelorMittal. 2015. *Duracorr®: Life-Cycle Cost-Effective 12% Chromium Stainless Steel*. ArcelorMittal USA, Chicago, IL. https://usa.arcelormittal.com/~/_media/Files/A/Arcelormittal-USA-V2/what-we-do/steel-products/plate-products/Duracorr-lifecycle.pdf.
- ASTM. 2014. *ASTM A1010/A1010M: Standard Specification for Higher-Strength Martensitic Stainless Steel Plate, Sheet, and Strip*. ASTM International, West Conshohocken, PA.
- ASTM. 2015a. *ASTM A588/A588M: Standard Specification for High-Strength Low-Alloy Structural Steel, up to 50 ksi [345 MPa] Minimum Yield Point, with Atmospheric Corrosion*. ASTM International, West Conshohocken, PA.
- ASTM. 2015b. *ASTM G101-024: Standard Guide for Estimating the Atmospheric Corrosion Resistance of Low-Alloy Steels*. ASTM International, West Conshohocken, PA.
- ASTM. 2015c. *ASTM E466-15: Standard Practice for Conducting Force Controlled Constant Amplitude Axial Fatigue Tests of Metallic Materials*. ASTM International, West Conshohocken, PA.
- ASTM. 2016. *ASTM E8/E8M: Standard Test Methods for Tension Testing of Metallic Materials*. ASTM International, West Conshohocken, PA.
- ASTM. 2017. *ASTM A709/709M: Standard Specification for Structural Steel for Bridges*. ASTM International, West Conshohocken, PA.
- ASTM. 2018. *ASTM A240/A240M: Standard Specification for Chromium and Chromium-Nickel Stainless Steel Plate, Sheet, and Strip for Pressure Vessels and for General Applications*. ASTM International, West Conshohocken, PA.
- ASTM. 2019. *ASTM A36/A36M: Standard Specification for Carbon Structural Steel*. ASTM International, West Conshohocken, PA.
- Barsom, J. M. and S. T. Rolfe. 1999. *Fracture and Fatigue Control in Structures: Applications of Fracture Mechanics*. Third Edition. ASTM International, West Conshohocken, PA.
- Cambier, S. M. N. 2014. *Atmospheric Corrosion of Coated Steel: Relationship between Laboratory and Field Testing*. PhD dissertation. Ohio State University, Columbus, OH.
- Chen, H., G. Y. Grondin, and R. G. Driver. 2007. Characterization of Fatigue Properties of ASTM A709 High Performance Steel. *Journal of Constructional Steel Research*, Vol. 63, No. 6, pp. 838–848.

- Cook, D. C. and R. D. Granata. 2002. *AISI High Performance Steel Corrosion Advisory Group NYS DOT Moore Drive Bridge: Coupon Exposure Project. Interim Report #1: Specimen Rack Construction and Installation*. American Iron and Steel Institute, Washington, DC.
- Cook, D. C., S. J. Oh, and H. E. Townsend. 1998. The Protective Layer Formed on Steels after Long-Term Atmospheric Exposure. *Corrosion* 98, March 22–27, San Diego, CA. <https://www.onepetro.org/download/conference-paper/NACE-98343?id=conference-paper%2FNACE-98343>.
- Crampton, D. D., K. P. Holloway, and J. Fraczek. 2013. *Assessment of Weathering Steel Bridge Performance in Iowa and Development of Inspection and Maintenance Techniques*. Iowa Department of Transportation, Ames, IA. [http://publications.iowa.gov/14956/1/Iowa Weathering Steel Final Report 2-21-2013.pdf](http://publications.iowa.gov/14956/1/Iowa_Weathering_Steel_Final_Report_2-21-2013.pdf)
- Daghash, S. M. and O. E. Ozbulut. 2017. Mechanical Evaluation of Corrosion-Resistant Steel Plates for Bridge Girder Fabrication. *Structures Congress 2017*, April 6–8, Denver, CO. pp.494–505.
- Ebrahimi, N., J. Zhang, B. Baldock, and D. Lai. 2018. Galvanic Corrosion Risk Assessment of Bolt Materials in Contact with ASTM A1010 Steel Bridges. *Corrosion* 2018, April 15–19, Phoenix, AZ.
- FHWA. 2011. *Improved Corrosion-Resistant Steel for Highway Bridge Construction*. FHWA-HRT-11-061. TechBrief. Federal Highway Administration, Research, Development, and Technology, Turner-Fairbank Highway Research Center, McLean, VA.
- FHWA. 2016. *Status of The Nation's Highways, Bridges, and Transit: Conditions & Performance*. Report to Congress. Federal Highway Administration and Federal Transit Administration, Washington, DC.
- Fletcher, F. B. 2005. Corrosion of Weathering Steels. In *ASM Handbook*, Vol. 13B, pp. 28–34.
- Fletcher, F. B. 2011. *Improved Corrosion-Resistant Steel for Highway Bridge Construction*. FHWA-HRT-11-062. Federal Highway Administration, Research, Development, and Technology, Turner-Fairbank Highway Research Center, McLean, VA.
- Fletcher, F. B. and J.-C. Gagnepain. 2007. New Stainless Steels for Bridge Applications. 24th Annual International Bridge Conference: Bridging Continents... Sharing Ideas, June 4–6, Pittsburgh, PA.
- Fletcher, F. B., H. E. Townsend, and A. D. Wilson. 2003. Corrosion Performance of Improved Weathering Steels for Bridges. National Steel Bridge Alliance (NSBA) World Steel Bridge Symposium, November 19–21, Orlando, FL.
- Fletcher, F. B., A. D. Wilson, J. Strasky, J. N. Kilpatrick, T. Mlcoch, and J. S. Wrynski. 2005. Stainless Steel for Accelerated Bridge Construction. FHWA Accelerated Bridge Construction 2005 Conference, December 15–16, San Diego, CA.
- Francis, R. 2000. *Guides to Good Practice in Corrosion Control: Bimetallic Corrosion*. The National Physical Laboratory, Teddington, Middlesex, UK.
- Groshek, I. G. 2017. Corrosion Behavior of ASTM A1010 Stainless Steel for Applications in Bridge Components. MS thesis. Virginia Polytechnic Institute and State University, Blacksburg, VA.
- Kihira, H., S. Ito, and T. Murata. 1990. The Behavior of Phosphorous during Passivation of Weathering Steel by Protective Patina Formation. *Corrosion Science*, Vol. 31, pp. 383–388.

- Koch, G. H., M. P. H. Brongers, N. G. Thompson, Y. P. Virmani, and J. H. Payer. 2002. *Corrosion Costs and Preventive Strategies in the United States*. FHWA-RD-01-156. NACE International, Houston, TX.
- Kogler, R. 2015. *Steel Bridge Design Handbook: Corrosion Protection of Steel Bridges*. FHWA-HIF-16-002-Vol. 19. Federal Highway Administration, Office of Bridges and Structures, Washington, DC
- Liljas, M. and C. Ericsson. 2002. Fatigue Behaviour of Stainless Steel Welds. *AvestaPolarit Corrosion Management and Application Engineering*, Vol. 1/2, pp. 2–16.
- McDad, B., D. C. Laffrey, M. Dammann, and R. D. Medlock. 2000. *Performance of Weathering Steel in TxDOT Bridges*. Texas Department of Transportation, Houston, TX.
<https://steel.org/~media/Files/SMDI/Construction/Bridges%20-%20WS%20-%20Report%20-%20Performance%20of%20WS%20in%20TX%20DOT%20Bridges%20by%20B%20McDad%20-%202006-02-2000.pdf>.
- NACE International. 2012. *Corrosion Control Plan for Bridges: A NACE International White Paper*. NACE International, Houston, TX.
<https://sgcweb.s3.amazonaws.com/roadsbridges/s3fs-public/CorrosionControlPlanForBridges.pdf>.
- Nip, K. H., L. Gardner, C. M. Davies, and A. Y. Elghazouli. 2010. Extremely Low Cycle Fatigue Tests on Structural Carbon Steel and Stainless Steel. *Journal of Constructional Steel Research*, Vol. 66, No. 1, pp. 96–110.
- Riley, W. F., L. D. Sturges, and D. H. Morris. 2007. *Mechanics of Materials*. Sixth Edition. John Wiley & Sons, Inc., Hoboken, NJ.
- Seradj, H. 2010. Weldability of ASTM A1010 Steel. *Proceedings of the 8th International Conference on Short and Medium Span Bridges*. August 3–6, Niagara Falls, Ontario, Canada.
- . 2015. Oregon’s ASTM A 1010 Bridges. Iowa DOT A1010 Steel Workshop, March 18, Ames, IA.
https://iowadot.gov/bridge/A1010/Presentations/A1010_Construction_IOWA_2015.pdf.
- Via, W. F., Jr. and K. N. Harrop. 2017. Virginia’s Initial Experience with an ASTM A1010 Plate Girder Bridge. VTCA - Spring Conference, April 6, Hampton, VA.
https://www.vtca.org/wp-content/uploads/2017/04/Presentation_sc17_harrop.pdf.

**THE INSTITUTE FOR TRANSPORTATION IS THE FOCAL POINT FOR TRANSPORTATION
AT IOWA STATE UNIVERSITY.**

InTrans centers and programs perform transportation research and provide technology transfer services for government agencies and private companies;

InTrans contributes to Iowa State University and the College of Engineering's educational programs for transportation students and provides K–12 outreach; and

InTrans conducts local, regional, and national transportation services and continuing education programs.



**IOWA STATE
UNIVERSITY**

Visit InTrans.iastate.edu for color pdfs of this and other research reports.